International Journal of Earth Sciences (2024) 113:1529–1548
https://doi.org/10.1007/s00531-024-02452-4

ORIGINAL PAPER

Geochemistry and petrology of metapyroxenite and metagabbro associated with Neoproterozoic serpentinites in the Arabian-Nubian Shield: fragments of a fore-arc ophiolite

Bassam A. Abuamarah[1] · Amany M. A. Seddik[2] · Mokhles K. Azer[3] · Simon A. Wilde[4] · Mahmoud H. Darwish[2]

Received: 9 April 2024 / Accepted: 7 August 2024 / Published online: 23 August 2024

Abstract

The dismembered ophiolites in the Wadi Al-Barramiya area, Central Eastern Desert of Egypt, are one of a series of Neoproterozoic ophiolites present in the Arabian-Nubian Shield. Here we present new fieldwork, whole-rock geochemical data, and mineral chemistry of metapyroxenite and metagabbro associated with the Al-Barramiya ophiolite in order to constrain its nature and tectonic setting; in particular whether the ophiolite was formed in a subduction or non-subduction setting. The rocks selected were obtained from the mantle section (serpentinized peridotite), an ultramafic (pyroxenite) and the crustal section (metagabbro). The serpentinized peridotite is altered to talc carbonate and listvenite, and associated with magnesite. Pyroxenite occurs as irregular coarse-grained lenses of websterite and olivine websterite within the serpentinite and occurs adjacent to the ophiolitic metagabbro. The metagabbros form scattered allochthonous masses of various sizes that are distributed across the area. The ophiolitic rocks are metamorphosed from greenschist to lower amphibolite facies. Locally, fresh relicts of olivine and Cr-spinel can be found in the serpentinite, whereas pyroxenite has fresh relicts of olivine, clinopyroxene and Cr-spinel. Cr-spinel in the metapyroxenite is zoned, with Al_2O_3, Cr_2O_3 and MgO decreasing and FeO_t increasing from cores to rims, reflecting the effects of metamorphism that selectively removed the now-depleted components. The metagabbros are characterized by enrichment in large-ion lithophile elements (LILE) over high field strength elements (HFSE) and are tholeiitic with a calc-alkaline affinity. The high Cr# (0.63–0.75) of fresh Cr-spinel relicts in the metapyroxenite, together with their low TiO_2 contents (0.04–0.24 wt%), indicate that this rock is similar to highly refractory ultramafic rocks that evolved in a fore-arc setting. This is supported by the high forsterite content (Fo = 0.91–0.93) of fresh olivine and high Mg# (0.93–0.95) of fresh clinopyroxene. Clinopyroxenes in the metapyroxenite and metagabbro have the chemical characteristics of boninite, confirming the fore-arc setting.

Keywords Arabian-Nubian Shield · Al-Barramiya ophiolite · Metagabbro · Metapyroxenite · Fore-arc mantle

Introduction

The Arabian-Nubian Shield (ANS) ophiolites are considered to be thrust sheets of oceanic lithosphere that were tectonically obducted onto the continental margin during closure of the Mozambique Ocean (Stern et al. 2004; El Bahariya 2018; Abuamarah 2020; Abdel-Karim et al. 2021; Moussa et al. 2022; Abuamarah et al. 2023; Ali et al. 2023). The ophiolites are widely distributed along major shear zones in both the central and southern sectors of the Eastern Desert of Egypt (Fig. 1). The complete ophiolitic sequence of the Egyptian ophiolites consists of a mantle unit of serpentinized peridotite accompanied by pyroxenite, overlain by a Moho transition zone and a crustal section composed of layered and isotropic gabbro, sheeted dykes, and pillowed

✉ Bassam A. Abuamarah
babuamarah@ksu.edu.sa

[1] Department of Geology and Geophysics, King Saud University, 11451 Riyadh, Saudi Arabia

[2] Geology Department, Faculty of Science, New Valley University, El-Kharga 72511, Egypt

[3] Geological Sciences Department, National Research Centre, Cairo, Egypt

[4] School of Earth and Planetary Sciences, Curtin University, Perth, WA 6845, Australia

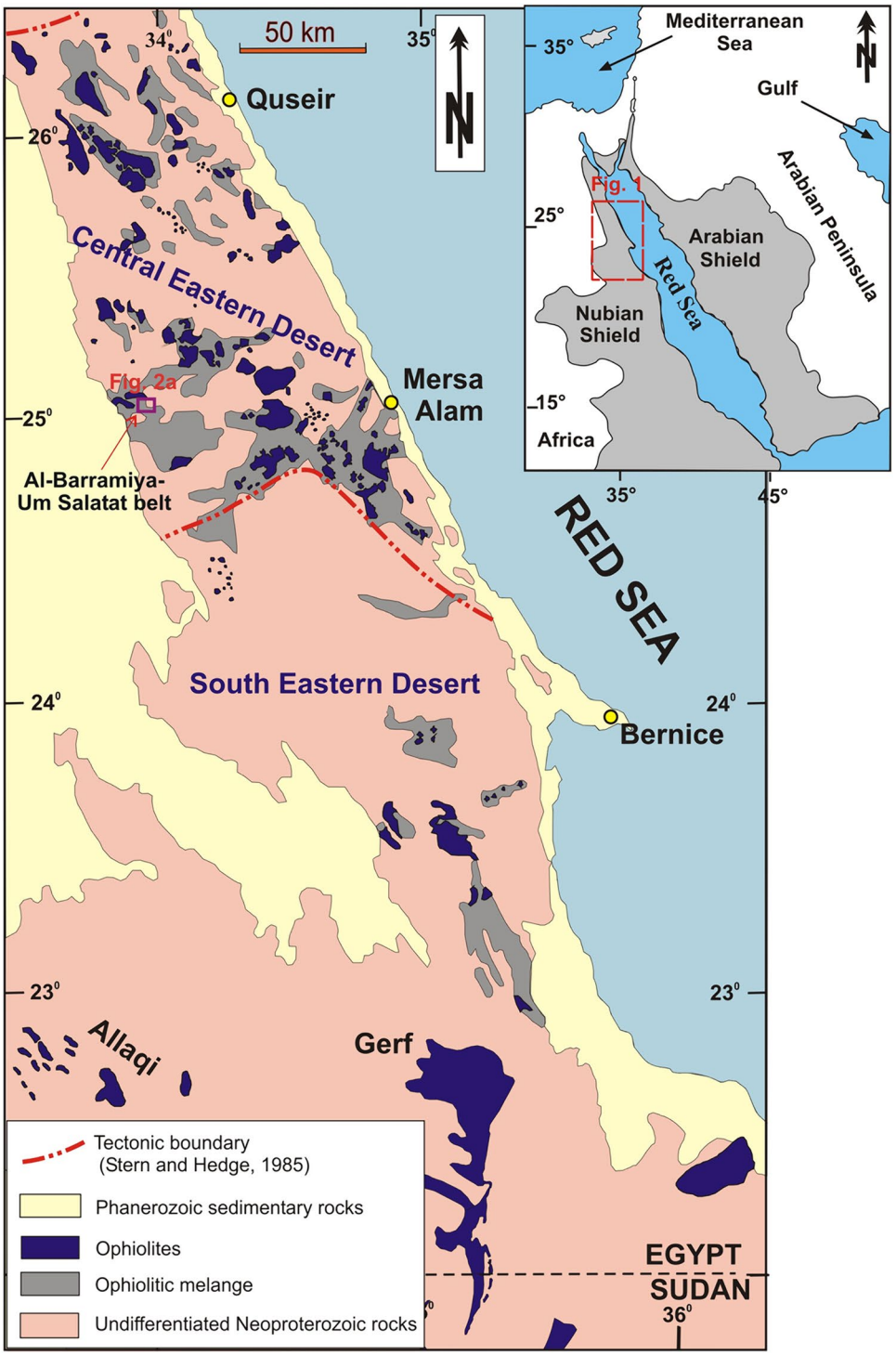

Fig. 1 Map of the Eastern Desert of Egypt [modified after Shackleton (1994)], showing distribution of ophiolitic rocks and location of Fig. 2; the insert map shows the location of Fig. 1 within the Arabian/Nubian Shield

metabasalt, with local pelagic sediments (e.g., El Sharkawy and El Bayoumi 1979; Abd El-Rahman et al. 2009a, b; Basta et al. 2011). Most of the Egyptian ophiolites are dismembered and lack one or more of these distinctive lithologies due to their obduction and subsequent deformation (Azer and Stern 2007; Akaad et al. 1997; El Bahariya 2006, 2018; Azer et al. 2013; Gahlan et al. 2021; Moussa et al. 2021). The ophiolitic mélanges in the Eastern Desert have been classified, based on their mode of occurrence, into tectonic mélange, olistostrome and olistostromal mélange (El Bahariya 2008; 2012).

Previous geological and petrological studies on the ophiolitic rocks at Al-Barramiya were focused mainly on the serpentinized peridotite and its alteration products (e.g., Zohier

and Lehmann 2011; Ali-Bik et al. 2012; Salem et al. 2012; Khedr and Arai 2017; Ali et al. 2020), whereas less attention has been given to the metapyroxenite and metagabbro. Therefore, the spatial and petrogenetic relationships between them and other ophiolitic components are the focus of the present research. Fieldwork and petrographical studies, together with mineral and whole-rock chemical data, are herein presented for the metapyroxenite and metagabbro to constrain their tectonic environment with respect to whether or not that formed in a subduction setting.

Geological setting

Ophiolites and ophiolitic mélanges are important rock units in the Al-Barramiya district and are a characteristic component of the Neoproterozoic rocks in the ANS (Zohier and Lehmann 2011; Ali et al. 2020). The area under investigation, Wadi Al-Barramiya, lies between latitudes 25° 04′ 15″ and 25° 06′ 15″ N and longitudes 33° 45′ and 33° 49 E and is located on the northern side of the Idfu-Mersa Alam Road, midway between Idfu and Mersa Alam (Figs. 1, 2): Idfu is located outside the mapped area to the west on the River Nile. Al-Barramiya forms the northeast part of the east-northeast trending Barramiya-Um Salatit ophiolitic belt and is characterized by a moderate relief with surface outcrops of Neoproterozoic rock units consisting of ophiolites, island-arc assemblages, metagabbro-diorite complexes and late intrusive granitic rocks, as well as Nubian sandstone of Cretaceous age (Fig. 2). Ophiolitic rocks in the area comprise extensively serpentinized peridotite, metagabbro, lenses of coarse-grained metapyroxenite, talc carbonate, magnesite and listvenite. Exotic ophiolitic blocks and fragments of serpentinized peridotite, metapyroxenite and metagabbro are dispersed in a sheared matrix of metasedimentary rocks forming ophiolitic mélange with an ENE-trending foliation.

Serpentinite is the most abundant rock type in the ophiolite and all serpentinite masses have tectonic contacts and

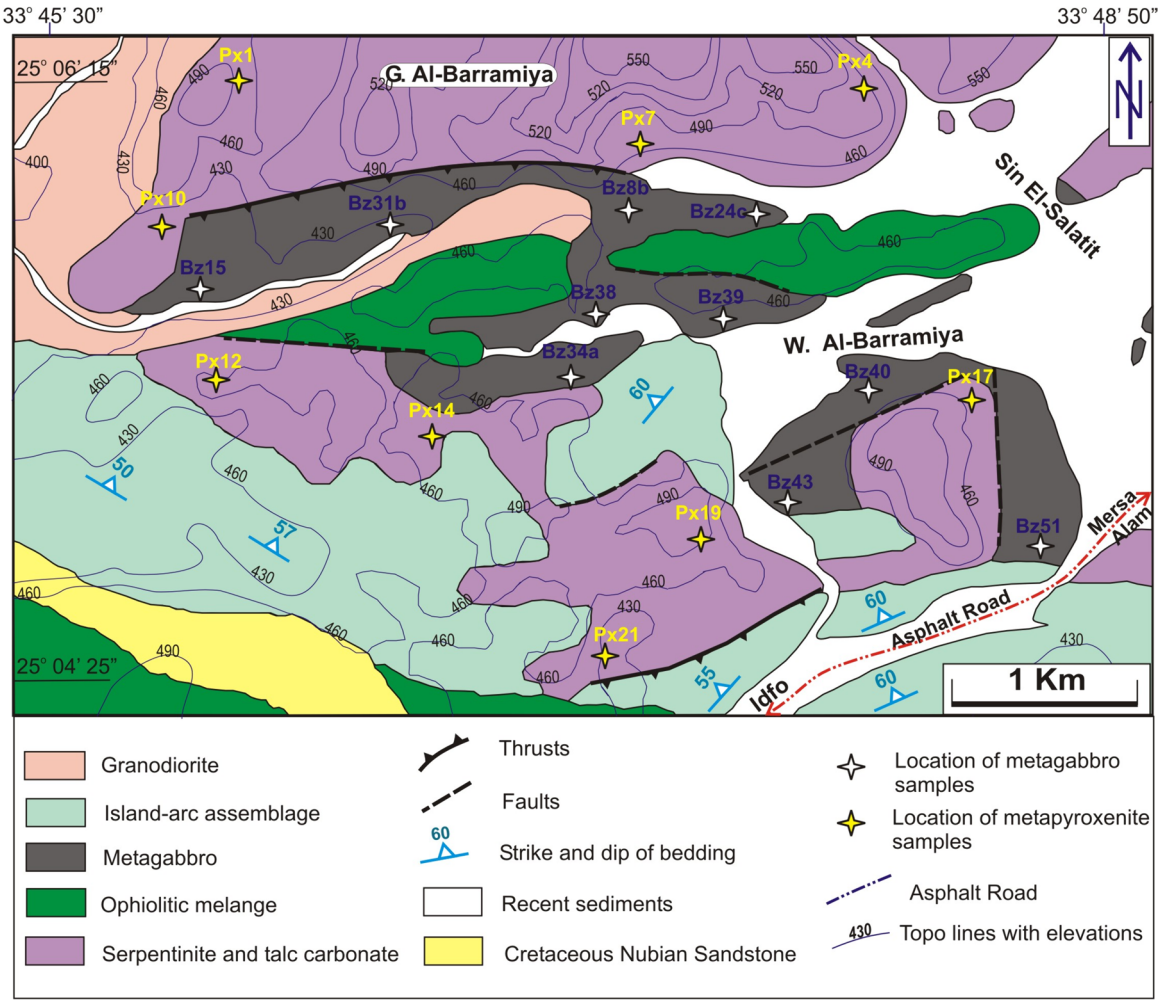

Fig. 2 Detailed geological map of the study area—Barramiya et al. [modified after Said (2006)]

have undergone strong brecciation and shearing. They occur as large thrust sheets forming topographic ridges which are elongated in a general ENE–WSW direction, concordant with the foliation in the surrounding matrix. They are commonly massive, but along fault planes and shear zones they are strongly carbonated and altered to talc carbonate, magnesite and listvenite. The contacts between talc carbonates and the parent serpentinites can be gradational, but are commonly sharp, with lenses of serpentinite set in talc carbonate (Fig. 3a). Some lenses of coarse-grained metapyroxenite are also present within serpentinite (Fig. 3b), especially at Sin El-Salatit (Fig. 2).

The talc carbonate rocks range in color from creamy white to light grey to yellowish-white or buff, and are characterized by cavernous weathering. Veinlets, nodules and irregular lenses of magnesite are observed in the sheared serpentinites and talc-rich rocks (Fig. 3c). The veinlets are generally orthogonal to the foliation in the talc-rich bodies.

Listvenite is infrequent in the study area, occurring as reddish-brown ridges, and as irregular lenses and masses along shear zones and fault planes. It forms positive relief features because of its resistance to weathering. Some listvenite outcrops have a porous texture as a result of supergene oxidation (Gahlan et al. 2018). Locally, listvenite is brecciated and fractured, with fractures filled with carbonate veinlets and fine quartz ribbons.

Ophiolitic metagabbros occur as scattered masses distributed throughout the ophiolitic mélange or as large masses and small hillocks that locally overlie serpentinite. The metagabbro is mostly grayish-green to black in color. A few pegmatitic gabbro (appinite) masses are present within more isotropic metagabbro. Some metagabbros are sheared (Fig. 3d) and overthrust by serpentinites. Abundant veins of carbonate, quartz and epidote cut the metagabbro. In the northern part of the study area (Fig. 2), the metagabbros are intruded by syn- to late-orogenic granodiorite.

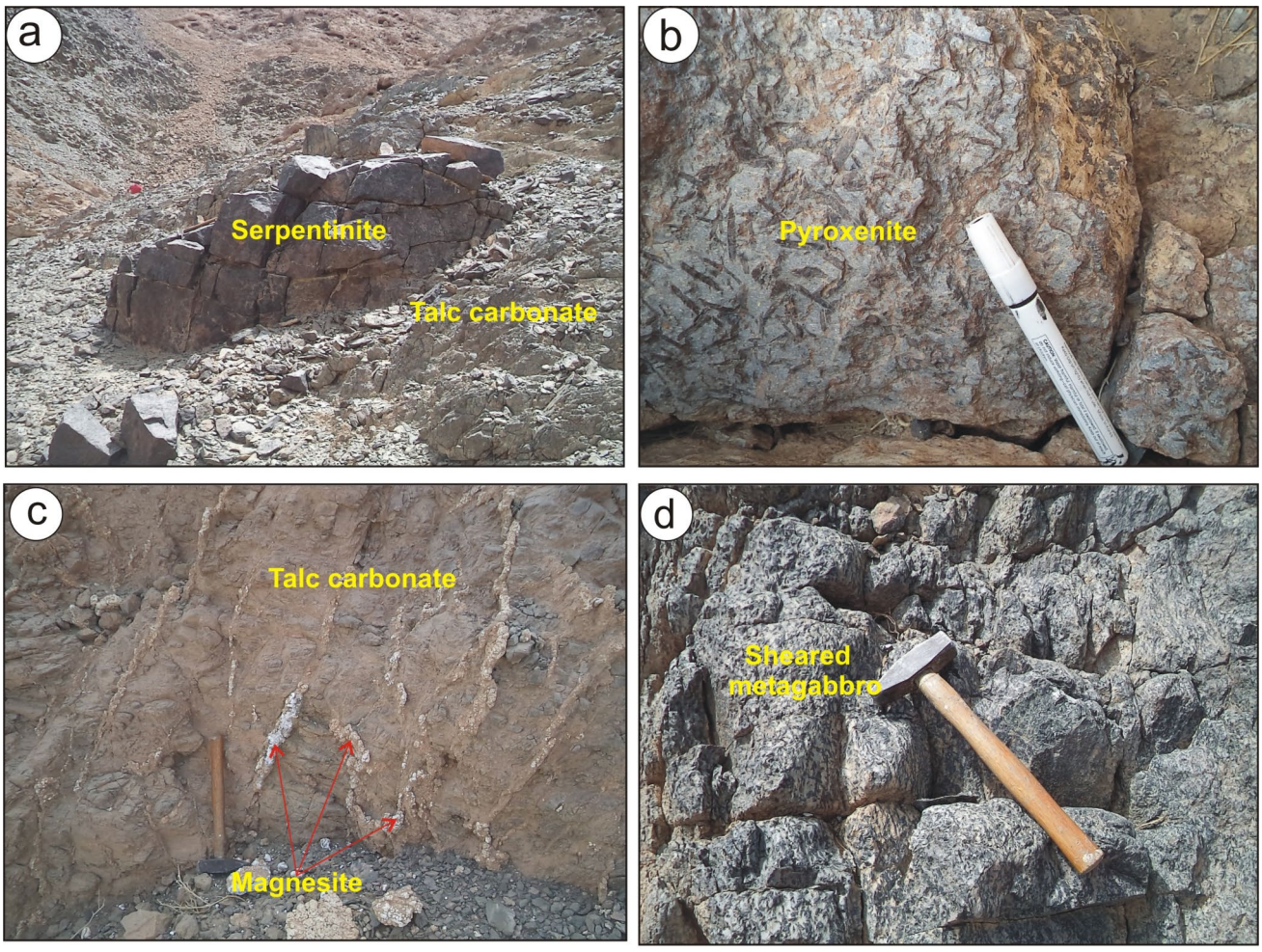

Fig. 3 Field photographs of **a** serpentinite body within talc carbonates; **b** lens of coarse-grained pyroxenite (sample no. Px14); **c** veinlets of magnesite in talc-rich rocks and **d** sheared metagabbro (sample no. Bz51)

The island-arc assemblages are widely distributed in the region and have thrust contacts with the ophiolitic rocks, especially with mélange and serpentinite. These rocks include metavolcanics, volcaniclastics and metasediments. All of the ophiolitic units and the island-arc assemblages are intruded by syn- to late-orogenic granodiorite. The Cretaceous Nubian sandstone unconformably overlies the Precambrian rocks in the western part of the mapped area (Fig. 2). It represents the base of the Phanerozoic sedimentary succession that extends westward towards the Nile Valley. It occurs either as continuous or separate small outcrops and is characterized by conspicuous, nearly horizontal beds with some cross-bedding.

Petrography

Serpentinite

Serpentinites are fine-grained and massive, but are locally sheared. They consist mainly of antigorite and lizardite, together with carbonate, talc, chlorite, opaque minerals and subordinate relicts of olivine and Cr spinel. Using Raman spectroscopy, antigorite was identified as the main serpentine mineral, with minor chrysotile occurring as fibrous lamellae or filling veinlets. The presence of bastite replacing orthopyroxene, as well as a more uniform mesh texture (Fig. 4a) indicates harzburgite and dunite protoliths, respectively. Fresh relicts of olivine also occur dissected by serpentine veinlets (Fig. 4b) and locally contain inclusions of Cr-spinel. Kink banding is observed in some olivine crystals. Magnesite is the main carbonate, with minor calcite, and occurs as rare crystals, patches or veinlets cutting through the serpentine matrix. Cr-spinel and magnetite are the main opaque minerals, together with minor sulphides. Cr-spinel is subhedral to anhedral, and has distinct zoning in some larger crystals. Magnetite forms disseminated crystals and as rims around olivine and Cr-spinel grains. Talc occurs in a few samples as anhedral patches and aggregates, and is colorless to very light brown. Chlorite forms aggregates of fine anhedral flakes or as a crust developed around Cr-spinel. Sulfides are present as minute crystals of pyrite and chalcopyrite.

Metapyroxenite

Metapyroxenite forms lenses within serpentinite and has undergone variable degrees of serpentinization. It consists mainly of clinopyroxene (> 90%) with minor plagioclase, together with trace amounts of olivine, magnetite and Cr-spinel. The clinopyroxene forms anhedral tabular crystals that are strongly altered along their rims to serpentine, secondary amphibole, chlorite, carbonate or talc, with a few relicts of primary clinopyroxene (Fig. 4c). The outlines of completely altered pyroxene crystals can be identified from the alignment of iron oxides along the cleavage planes. Some fresh relicts of clinopyroxene have exsolution lamellae and contain anhedral grains of serpentine after olivine. Olivine grains are mainly interstitial to large clinopyroxene crystals, but also occur as inclusions in clinopyroxene, or within serpentinized domains (Fig. 4d). Secondary amphibole forms bundles of tremolite-actinolite that replaces clinopyroxene along the margins, cleavage or cracks. Serpentine is mostly found as thin crusts around clinopyroxene or replacing it along cracks. Carbonates occur as patches and veinlets of calcite cutting through the rock. Opaque minerals are magnetite and Cr-spinel with the former commonly oriented parallel to the cleavage planes of clinopyroxene. Cr-spinel occurs as anhedral crystals that are altered along their margins to ferritchromite and Cr-magnetite (Fig. 4e).

Metagabbro

Metagabbro is essentially composed of plagioclase, amphibole and pyroxene relicts. Apatite, zircon, titanite and opaques are accessory minerals, whereas chlorite, epidote, sericite, calcite and kaolinite are secondary minerals. An ophitic to sub-ophitic texture is preserved in a few samples. Plagioclase is the most common mineral and occurs as large subhedral tabular crystals that show intense alteration to epidote and sericite, especially in the cores (Fig. 4f). The amphibole comprises hornblende and tremolite-actinolite, with the latter representing pesudomorphs after pyroxene or alteration of hornblende. Hornblende forms long prismatic crystals and aggregates with a pale to darker green pleochroism. Tremolite-actinolite occurs as fibers with ragged edges or as fine aggregates that form bundles (Fig. 4g).

Clinopyroxene is extensively altered to green hornblende, tremolite-actinolite or chlorite. A few remnants of fresh clinopyroxene occur surrounded by amphibole (Fig. 4h). Chlorite forms irregular flakes due to alteration of pyroxene and amphibole.

Secondary epidote, sericite, kaolinite and calcite occur as anhedral granular aggregates replacing plagioclase. Some carbonate forms patches and veinlets. The opaque mineral content is variable and ranges between 3 and 6 vol%. It mainly consists of Fe-Ti oxides with minor sulfides. The former occur as separate crystals or as fine aggregates associated with the altered mafic minerals, and mainly consist of ilmenite, with rare magnetite. Sulphides include both pyrite and chalcopyrite. Some magnetite is altered to goethite, whereas chalcopyrite is altered to covellite. Apatite occurs as small prismatic crystals in amphibole.

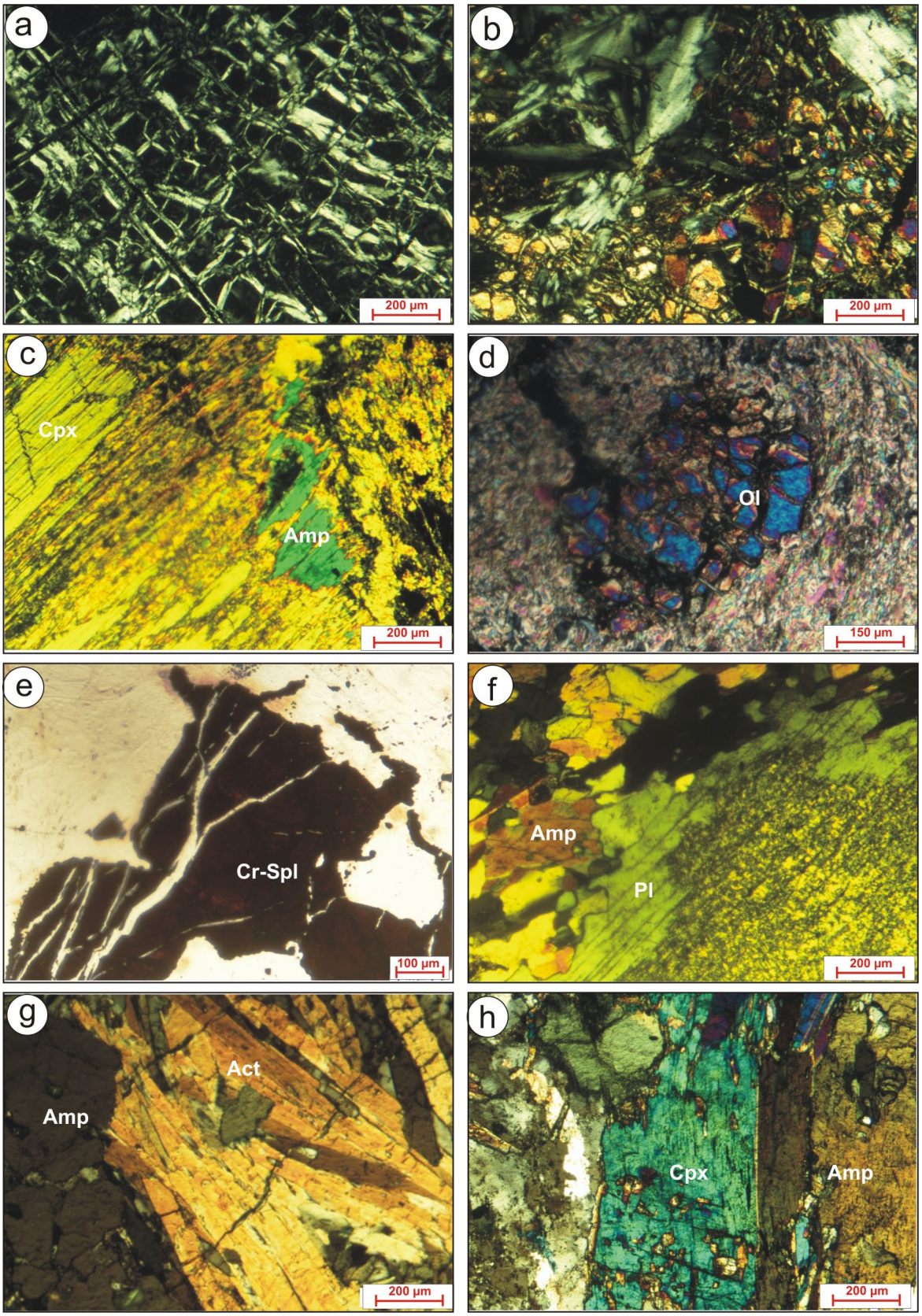
a
200 µm
b
200 µm
c
Cpx
Amp
200 µm
d
Ol
150 µm
e
Cr-Spl
100 µm
f
Amp
Pl
200 µm
g
Act
Amp
200 µm
h
Cpx
Amp
200 µm

◂**Fig. 4** Photomicrographs of metapyroxenite and metagabbro from the Al-Barramiya ophiolite (all photomicrographs are cross-polarized transmitted light, except (**e**), which is in plane polarized light). **a** Serpentine mesh texture after olivine in serpentinite; **b** fresh relict of olivine in highly serpentinized peridotite; **c** clinopyroxene altered to amphibole and other secondary minerals, but with some fresh relicts; **d** relicts of olivine in highly-serpentinized metapyroxenite (sample no. Px17); **e** cracked, anhedral crystal of Cr-spinel altered along the margins to ferritchromite and Cr-magnetite (sample no. Px10); **f** plagioclase showing intense alteration to secondary minerals in the core (sample no. Bz8b); **g** bundles of fibrous secondary amphibole, with hornblende relicts (sample no. Bz43); and **h** fresh clinopyroxene within amphibole in metagabbro (sample no. Bz15)

Analytical techniques

Mineral chemical analyses were obtained from carbon-coated polished thin-sections using a JEOL JXA-8530F field-emission electron microprobe (EMPA) housed at the Department of Earth Sciences, University of Western Ontario, Canada. Operating conditions were 20 kV probe current; 40–60 nA accelerating voltage; 1–2 µm diameter beam; and counting time of 5–10 s. Natural and synthetic mineral standards were used for calibration, and a ZAF matrix correction routine program was applied. The standards were orthoclase for K, albite for Na and Al, anorthite for Ca, rutile for Ti, zircon for Si, forsterite for Mg and fayalite for Fe. Calculation of cations in the structure of the analyzed minerals was performed using Excel sheets and Minpet software. The mineral formulae were normalized to a specific number of oxygens, depending on each mineral as atoms per formula unit (a.p.f.u.).

Based on the petrographic studies, 19 samples were selected out of a total of sixty for chemical analysis at Northwest University, Xi'an, China. A portion of the powdered samples was heated at 1000 °C in an oven for 50 min to determine the Loss on Ignition (LOI). Another portion of the powdered sample was analyzed by X-ray fluorescence (XRF, Rigaku RIX2100) by mixing 0.7 g of sample, 0.3 g LiF, 0.4 g NH_4NO_3, 3.6 g $Li_2B_4O_7$, and 2–3 drops of 1.5% (w/w) LiBr solution. This mixture was melted in a non-wetting precious metal crucible and poured into a glass disk. In addition, 50 mg of sample powder was mixed with $HClO_4$, HNO_3 and HF and digested at 190 °C for 48 h in steel bombs with polytetrafluoroethylene sleeves. After drying, the residues were taken up in 80 mL of 2% HNO_3 with 10 µg/g of Rh as an internal standard. These solutions were analyzed by ICP-MS (Agilent 7500a) for trace and rare earth elements (REEs). The analytical protocol was monitored using international rock standards (BCR-2, BHVO-1 and AGV-1). The analytical precision, based on sample replicates, was better than 1% for major oxides and 5–10% for REE and trace elements.

Mineral chemistry

Metapyroxenite

Four different mineral phases (olivine, clinopyroxene, Cr-spinel and serpentine) were analysed from two metapyroxenite samples (BZ9 and UM13) by electron microscopy (EM). Fresh relicts of olivine were analyzed and their chemical compositions and calculated structural formulae are listed in supplementary table ST1. All the analyzed olivine crystals are unzoned forsterite and show little variability in their composition, with SiO_2 ranging from 40.29 to 41.21 wt%, MgO from 49.39 to 51.23 wt%, and NiO between 0.41 and 0.48 wt%, with negligible amounts of TiO_2 (< 0.02 wt%), Al_2O_3 (< 0.04 wt%), Cr_2O_3 (< 0.07 wt%), and CaO (< 0.05 wt%). Olivine has a high forsterite content of Fo = 0.91–0.93 and NiO content of 0.41–0.48 wt%, similar to mantle olivine (Takahashi et al. 1987). On the olivine mantle array diagram, the olivine mostly plots in the mantle olivine array, and all plot in the field of the ANS ophiolites (Fig. 5a).

The chemical composition of fresh pyroxene relicts (Supplementary table ST2) are homogeneous and also show limited compositional variation. According to the classification of Morimoto et al. (1988), the pyroxenes in the metapyroxenite plot mainly in the diopside field (Fig. 5b). They have 0.37–1.12 wt% Cr_2O_3 and Al_2O_3 contents of 1.02–2.68 wt%, confirming their primary origin, because metamorphic clinopyroxenes have lower Cr_2O_3 (< 0.4 wt%) and Al_2O_3 (< 0.5 wt%) contents (Nozaka 2010). The CaO content is in the range of 21.82–24.21 wt% and TiO_2 contents are lower than 1 wt%, which is characteristic to non-alkaline rocks (Le Bas 1962). The Mg# is high (0.93–0.95 wt%) and similar to that of ophiolitic ultramafic rocks in the ANS (Obeid et al. 2016; Azer et al. 2019; Gahlan et al. 2020), as well as worldwide (Parlak et al. 2000; 2013; Allahyari et al. 2014). On the Al_2O_3 vs. SiO_2 discrimination diagram of Franz and Wirth (2000), the metapyroxenite clinopyroxenes plot as subalkaline (Fig. 5c).

The chemical composition and structural formulae of Cr-spinel and its alteration products are given in supplementary table ST3. It shows compositional zoning, with fresh Cr-spinel cores and an outer zone of ferritchromite that is commonly altered to an outer rim of Cr-magnetite. Going from core to rim, $FeO_{(t)}$ content increases, while Al_2O_3, Cr_2O_3 and MgO decrease. On the Cr–Al–Fe^{3+} diagram (Fig. 5d) the fresh cores plot along or near the Al-Cr line whereas the altered rims plot along the Cr-Fe^{3+} line, indicating the loss of both Cr_2O_3 and Al_2O_3 and a consequent increase in the Fe_2O_3 content as a result of metamorphism under hydrothermal conditions (Barnes

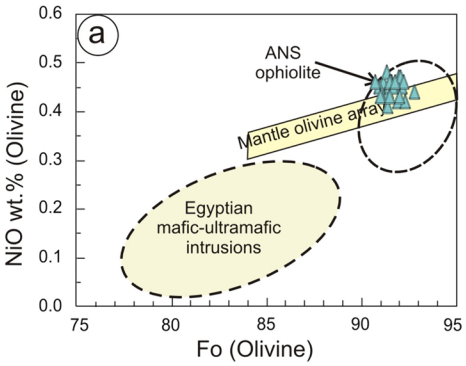
a
ANS ophiolite
Mantle olivine array
Egyptian mafic-ultramafic intrusions
NiO wt.% (Olivine)
Fo (Olivine)

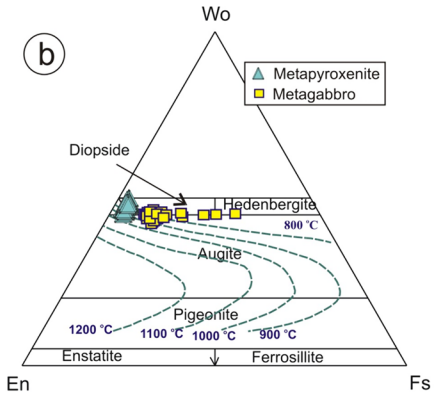
b
Wo
Metapyroxenite
Metagabbro
Diopside
Hedenbergite
800 °C
Augite
Pigeonite
1200 °C
1100 °C
1000 °C
900 °C
Enstatite
Ferrosillite
En
Fs

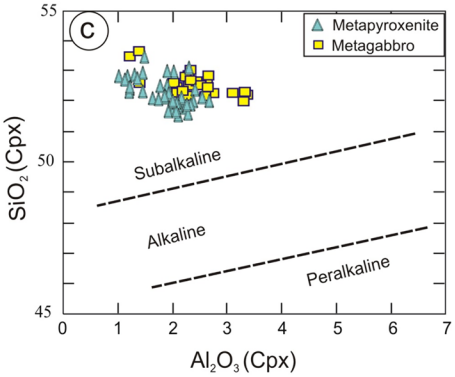
c
Metapyroxenite
Metagabbro
Subalkaline
Alkaline
Peralkaline
SiO2 (Cpx)
Al2O3 (Cpx)

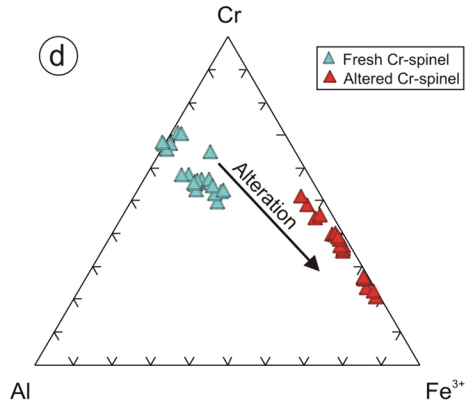
d
Cr
Fresh Cr-spinel
Altered Cr-spinel
Alteration
Al
Fe3+

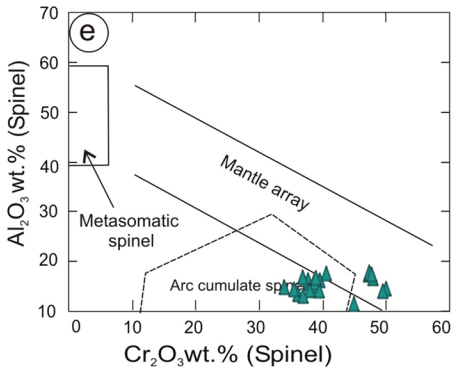
e
Al2O3 wt.% (Spinel)
Mantle array
Metasomatic spinel
Arc cumulate spinel
Cr2O3wt.% (Spinel)

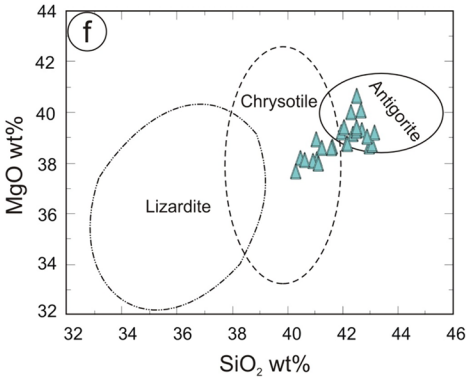
f
MgO wt%
Chrysotile
Antigorite
Lizardite
SiO2 wt%

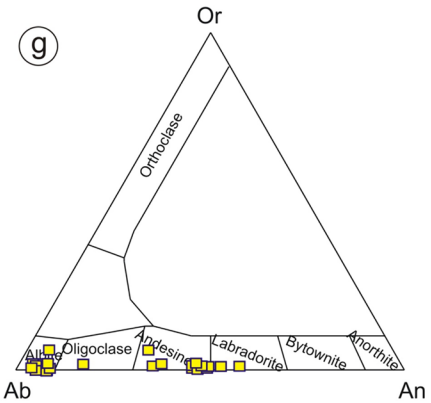
g
Or
Orthoclase
Albite
Oligoclase
Andesine
Labradorite
Bytownite
Anorthite
Ab
An

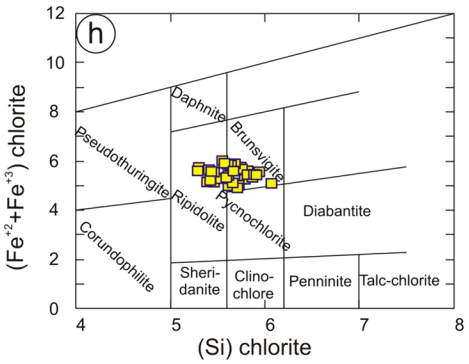
h
(Fe+2+Fe+3) chlorite
Daphnite
Brunsvigite
Pseudothuringite
Ripidolite
Pycnochlorite
Diabantite
Corundophilite
Sheri-danite
Clino-chlore
Penninite
Talc-chlorite
(Si) chlorite

◂**Fig. 5** **a** NiO vs. Fo showing where fresh olivine relicts in metapyroxenite plot compared with the olivine mantle array (Takahashi et al. 1987), ophiolites of the ANS (Khalil et al. 2014; Gahlan et al. 2015, 2018; Obeid et al. 2016; Azer et al. 2019), and layered intrusions of the ANS (Helmy and Mahallawi 2003; Abd El-Rahman et al. 2012; Abdel-Halim et al. 2016; Azer et al. 2017; Gahlan et al. 2023); **b** En-Wo-Fs triangular diagram (after Morimoto et al. (1988), with isotherms after Lindsley (1983). showing where metapyroxenite and metagabbro from Al-Barramiya plot; **c** SiO_2 vs. Al_2O_3 diagram of Le Bas (1962) for clinopyroxene; **d** Cr–Al–Fe^{3+} plot of fresh and altered Cr-spinel. **e** Al_2O_3 vs. Cr_2O_3 diagram (after Franz and Wirth 2000), showing where fresh relicts of Cr-spinel plot; **f** MgO vs. SiO_2 classification diagram for serpentine polymorphs (Bahrambeygi et al. 2019); **g** Or–Ab–An ternary diagram (Deer et al. 1992) with analyzed feldspars plotted; and **h** classification diagram for chlorite-group minerals (Hey 1954)

2000; Proenza et al. 2004). The fresh Cr-spinel cores have Cr# (molar Cr/(Cr + Al)) ranging between 0.63 and 0.75, with an average of 0.67, and Mg# (molar Mg/(Mg + Fe^{2+})) ranging from 0.41 to 0.64, with an average of 0.56. Relative to fresh spinel cores, the altered rims have higher Cr# (0.90–0.96; av.0.93) and lower Mg# (0.11–0.52; av. 0.32). Generally, the fresh Cr-spinel cores have Al_2O_3 and Cr_2O_3 contents that are similar to those of Cr-spinel of mantle peridotite and most plot in or near the mantle array, but extending into the arc cumulate field (Fig. 5e).

The chemical composition and structural formulae of the serpentine minerals in the metapyroxenite are given in Supplementary table ST4. On the SiO_2 versus MgO diagram of Bahrambegi et al. (2019), they range from antigorite to chrysotile in composition (Fig. 5f).

Metagabbro

The metagabbro minerals include plagioclase, pyroxene, amphibole, chlorite and ilmenite. The chemical composition and structural formula of plagioclase are listed in Supplementary table ST5. They range in composition from labradorite to albite (Fig. 5g), with An contents varying from 57.20 to 4.07. The low anorthite content of some plagioclase is attributed to its albitization during metamorphism.

Fresh pyroxene relicts are rare, and their chemical composition and calculated structural formula are listed in Supplementary table ST6. They are calcic in composition and according to the classification of Morimoto et al. (1988), they mainly straddle the boundary between the diopside and augite fields and extend to hedenbergite in composition (Fig. 5b). On the SiO_2 vs. Al_2O_3 diagram of Le Bas (1962) for clinopyroxene, they plot in the subalkaline field (Fig. 5c), similar to the metapyroxenite crystals.

Amphiboles in the metagabbro include primary magmatic minerals (hornblende) and subsequent alteration products (tremolite-actinolite). Their chemical analyses and structural formulae are presented in Supplementary table ST7. According to the amphibole classification scheme of Hawthorne et al. (2012), they are calcic amphiboles; namely magnesio- to ferri-hornblende and actinolite.

Chlorite forms due to alteration of pyroxene and amphibole. Representative chemical analyses and the structural formula are given in Supplementary table ST8. They show limited variation in composition and, according to the scheme of Hey (1954), they are classified as brunsvigite and ripidolite (Fig. 5h).

Ilmenite is the main Fe-Ti oxide mineral in the metagabbro, and its representative chemical composition and structural formula are given in Supplementary table ST9. Chemically, it is homogenous and has low MgO contents indicating formation by low-grade metamorphism, after most MgO had been sequestered in other phases.

Whole-rock geochemistry

Nineteen representative samples of metagabbro (10 samples) and metapyroxenite (9 samples) from the ophiolitic rocks cropping out in the Al-Barramiya area were analyzed for their major oxides, trace and rare earth elements. The whole-rock chemical analyses are presented in supplementary table ST10. Some of the trace elements are below the detection limit of the analytical protocol used. Overall, the metapyroxenite samples have high LOI (4.21–5.24 wt%) compared with the metagabbro samples (2.37–4.01 wt%).

Metapyroxenite

The metapyroxenite samples have 47.72–51.30 wt% SiO_2, 0.08–0.16 TiO_2 wt%, 15.45–18.72 MgO wt%, 1.34–2.87 Al_2O_3 wt% and 15.83–19.88 CaO wt%. They have high concentrations of compatible elements (Supplementary table ST10), such as Cr (1120–2120 ppm), Ni (401–711 ppm), Co (67–91 ppm) and Sc (161–276 ppm). Due to the serpentinized nature of the metapyroxenite, the classification scheme based on modal percentages of olivine, clinopyroxene and orthopyroxene is unsuitable. Therefore, using the normative whole-rock composition (Supplementary table ST10), the metapyroxenite can be classified as websterite and olivine websterite, but very close to the clinopyroxenite field (Fig. 6a). On the SiO_2/MgO versus Al_2O_3 diagram (Bodinier and Godard 2003), the metapyroxenite samples plot as low-Al pyroxenite (Fig. 6d). On the primitive mantle (PM)-normalized trace element diagram, the metapyroxenite samples show positive peaks for Cs, Ba, U, Pb and Eu (Fig. 7a), with marked depletion in Rb, Nb, and Hf. In the chondrite-normalized REE diagram (Fig. 7b) the metapyroxenites show depletion in LREEs (3.52–5.69 ppm) and flat MREE to HREE patterns. They have (La/Sm)n = 0.35–0.39 and (La/Yb)n = 0.28–0.37. The depletion in LREEs is comparable

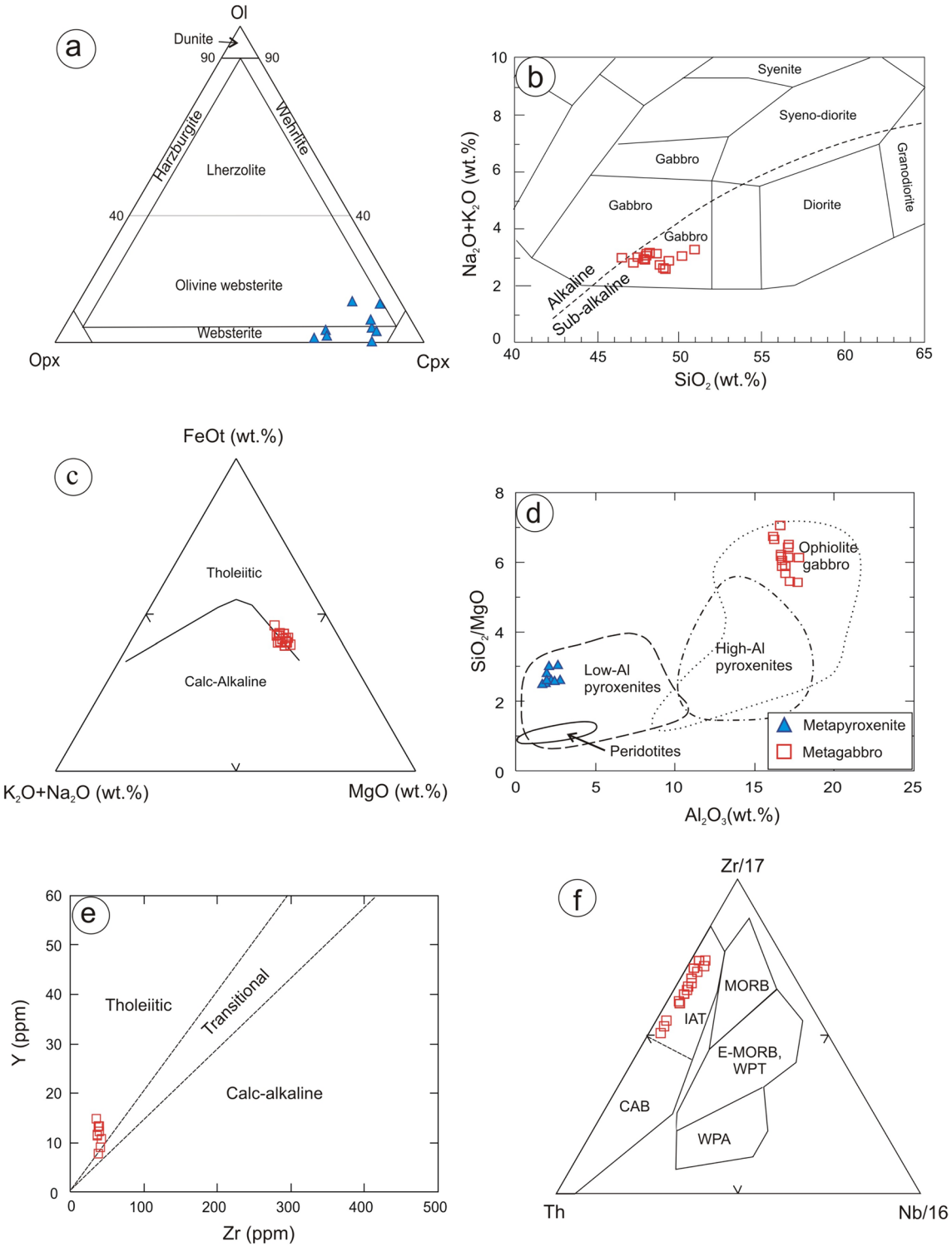

Fig. 6 **a** Metapyroxenites plotted in the Ol-Opx-Cpx normative composition diagram (after Coleman 1977); **b** Metagabbros plotted in the TAS diagram of Cox et al. (1979), adapted by Wilson (1989) for plutonic rocks; **c** Metagabbros plotted in the AFM diagram of Irvine and Baragar (1971); **d** metapyroxenites and metagabbros plotted in the SiO_2/MgO versus Al_2O_3 diagram (Bodinier and Godard 2003); **e** metapyroxenites and metagabbros plotted in the Y vs. Zr diagram after Barrett and McLean (1994); and **f** Metagabbros plotted in the Th–Zr–Nb ternary diagram, modified after Wood (1980)

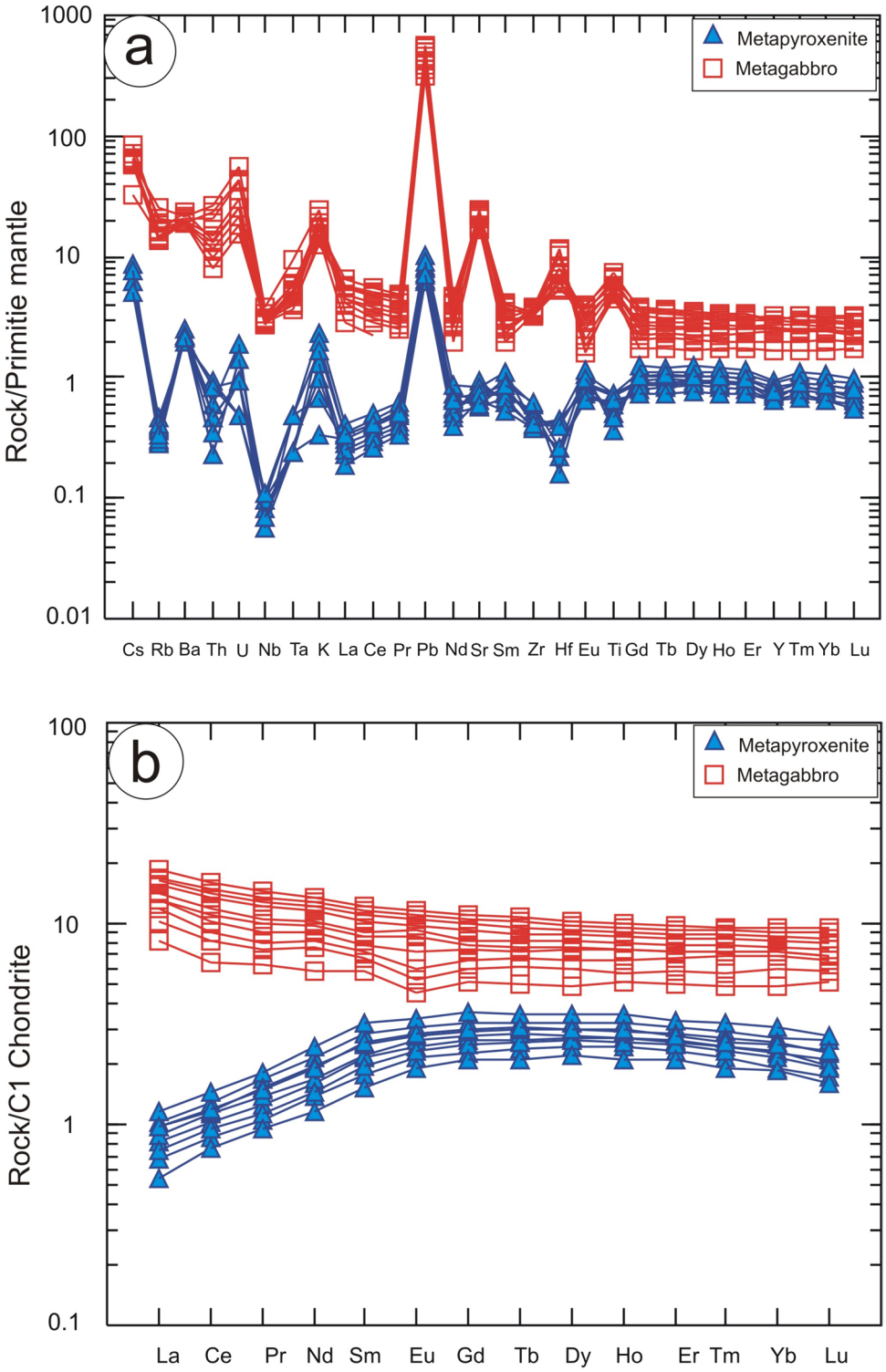

Fig. 7 **a** Primitive mantle-normalized trace element patterns for metapyroxenite and metagabbro from Al-Barramiya, and **b** chondrite-normalized rare earth element patterns for metapyroxenite and metagabbro; normalization values for **a** and **b** from McDonough and Sun (1995)

with other ophiolitic clinopyroxenites in the ANS (Gahlan et al. 2012).

Metagabbro

The metagabbro samples have slightly lower SiO_2 (46.50–50.87 wt%) and much lower MgO (7.34–8.73 wt%) contents than the metapyroxenite, but have higher Al_2O_3 (16.23–17.74 wt.%) and TiO_2 (0.98–1.62 wt.%) contents.

The whole-rock Mg# [molar Mg/(Mg + Fe^{2+})] ranges from 0.59 to 0. 76, lower than that in the metapyroxenite samples. They also have lower compatible elements (Supplementary table ST10), with (Cr = 111–182 ppm, Ni = 40–128 ppm, Co = 44–58 ppm, and Sc = 36–48 ppm). On the TAS discrimination diagram of Cox et al. (1979) (Fig. 6b), the samples plot in the field of gabbro with a slight spread into the sub-alkalic field. On the AFM diagram (Irvine and Baragar 1971), they straddle the boundary between the tholeiitic and calc-alkaline fields (Fig. 6c). On the SiO_2/MgO versus Al_2O_3 diagram (Bodinier and Godard 2003), the metagabbro samples plot within the ophiolitic gabbro field (Fig. 6d). On the Zr versus Y diagram, they plot in the tholeiitic field but extend down into the transitional field (Fig. 6e), whereas in the Th–Zr–Nb ternary diagram (Fig. 6f), they plot in the field of island-arc tholeiite.

The primitive mantle (PM)-normalized trace element patterns for the metagabbro are essentially similar to those of the metapyroxenite, but with higher total contents and stronger Pb enrichment (Fig. 7a). They show similar depletion in Rb and Nb, but contrast with the metapyroxenite in showing enrichment in Hf and Ti, but depletion in Eu. The positive Ti anomalies can be attributed to higher amounts of Fe-Ti oxide minerals in these samples. Both metapyroxenite and metagabbro samples have negative Nb anomalies similar to those of other ophiolitic metagabbros in the Eastern Desert of Egypt (Gahlan et al. 2015; Obeid et al. 2016). In the chondrite-normalized REE plot (Fig. 7b), they show slightly enriched LREEs, but with flat MREE to HREE patterns (Gd/Lu = 0.98–1.18) and $(La/Lu)_n$ = 1.50–1.88. They have weakly negative to slightly positive Eu anomalies [Eu/Eu^* = 0.84–1.07], indicating a general lack of plagioclase fractionation. Overall, the REE patterns of the Al-Barramiya metagabbro are similar to ophiolitic metagabbros elsewhere in the ANS (Gahlan et al. 2015; Obeid et al. 2016).

Discussion

Alteration and metamorphism

Most ophiolites in the Eastern Desert of Egypt are metamorphosed to greenschist or lower amphibolite facies (e.g., Khalil and Azer 2007; El Bahariya 2006, 2008, 2018; Farahat 2008; Boskabadi et al. 2017; Abuamarah et al. 2020, 2023). However, it remains controversial when metamorphism of the Egyptian ophiolites took place, i.e. whether it was during or after their emplacement in the continental crust. For the ophiolitic rocks in the Al-Barramiya area, it has been suggested that they underwent various degrees of post-magmatic alteration either by seafloor hydrothermal activity or during the obduction processes (Ali et al. 2020). Although some of the original igneous textures of the ophiolitic metagabbro are still preserved, the mineralogy has been largely altered, with the primary minerals (plagioclase, amphibole and pyroxene) altered to secondary/metamorphic ones (albite, epidote, tremolite/actinolite, chlorite and titanite). Data presented here indicates that the ophiolitic metagabbro at Al-Barramiya is rich in LILEs and Th, most likely as a result of element mobility during slab dehydration (Pearce and Peate 1995).

Mineral assemblages in most samples of serpentinite, metapyroxenite and metagabbro suggest that they underwent regional metamorphism under greenschist to amphibolite facies conditions (e.g., Suita and Streider 1996; Mellini et al. 2005; El Bahariya 2006; El Bahariya and Arai 2003; Azer et al. 2019; Whattam et al. 2022). Ferritchromite in the metapyroxenite is enriched in $FeO_{(T)}$ (49.43–75.26 wt%) and depleted in Al_2O_3 (0.42–2.43 wt%) and MgO (1.82–8.04 wt%), reflecting the increase in Fe_2O_3 and loss of Al_2O_3 and Cr_2O_3 due to metamorphism (Azer and Stern 2007). The alteration of Cr-spinel to ferritchromite possibly took place during the late magmatic stage, and continued later due to serpentinization (Gahlan et al. 2018). The presence of ferritchromite rims around fresh Cr-spinel cores with a sharp compositional change likely indicates upper greenschist to lower amphibolite facies metamorphism (Evans and Frost 1975; Suita and Streider 1996; Barnes and Roeder 2001; Mellini et al. 2005; Arai et al. 2006). This is supported by the chemical data of Cr-spinel in the metapyroxenite on the Cr-Fe^{3+}-Al triangular diagram (Fig. 8a), where fresh Cr-spinel relicts and ferritchromite rims plot mostly in the lower amphibolite facies field. Also, serpentinite is dominated by antigorite, with subordinate chrysotile, indicating serpentinization during heating and burial (Moody 1976; Deer et al. 1992), or retrograde formation of chrysotile followed by a second cycle of prograde recrystallization to antigorite. The dominance of antigorite over chrysotile in the serpentinite suggests formation at 400 – 600 °C during an early stage of serpentinization at depth (Evans 2010).

Petrogenesis and tectonic setting

Dilek and Furnes (2014) classified ophiolites simply into subduction-related and subduction-unrelated types. The former include fore-arc and back-arc supra-subduction zone and volcanic arc types, whereas the latter comprise continental margin, mid-ocean ridge and plume-types. Several studies have been dedicated to determining the origin and tectonic setting of the Egyptian ophiolites because they represent key components in constructing the geodynamic model for the Pan-African belt of the ANS. Unfortunately, the metamorphosed nature of the Egyptian ophiolites makes it more difficult to infer their tectonic setting. Indeed, a wide range of tectonic settings has been proposed for these rocks, ranging from mid-ocean ridge (e.g., Shackleton et al. 1980; Zimmer

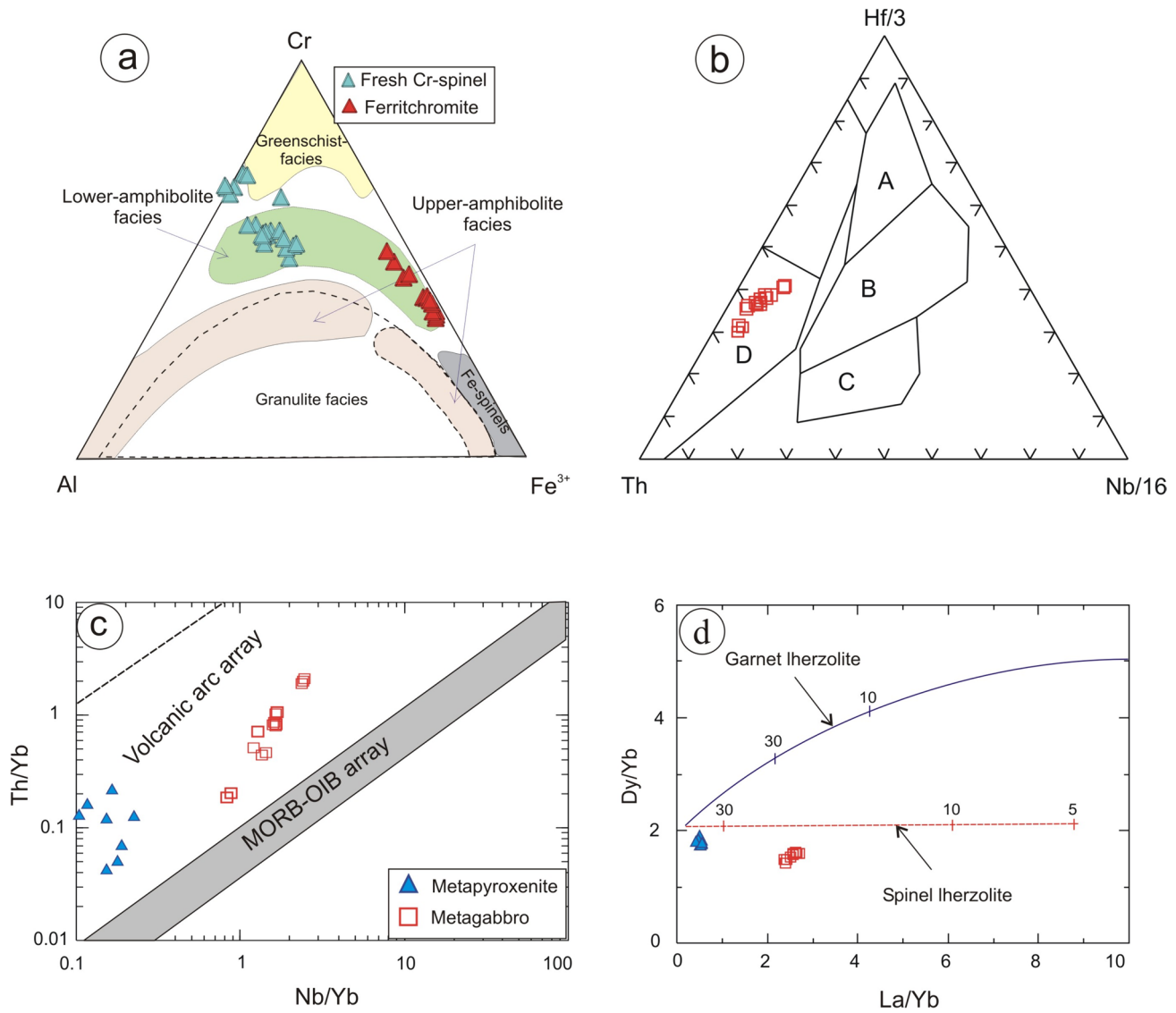

Fig. 8 **a** Cr–Fe^{3+}–Al^{3+} diagram for fresh and altered Cr-spinel in metapyroxenite; the fields of the different metamorphic facies from Purvis et al. (1972), Evans and Frost (1975) and Suita and Streider (1996); **b** Hf/3-Th-Nb/16 discrimination diagram after Wood (1980) for the Al-Barramiya metagabbro; A = N-MORB, B = enriched MORB and within-plate tholeiites, C = within-plate basalts and D = destructive plate basalts; **c** Th/Yb vs. Nb/Yb diagram after Pearce (2008) for the Al-Barramiya metagabbros and metapyroxenites; and **d** Dy/Yb vs. La/Yb diagram after Xu et al. (2001) for the metagabbros and metapyroxenites of the Al-Barramiya ophiolite

et al. 1995), to supra-subduction zone (fore-arc or back-arc setting) (e.g., Ahmed et al. 2001, 2012; Azer and Stern 2007; Ahmed 2013; Abdel-Karim et al. 2018). The Neoproterozoic ophiolites of Egypt have also been classified into high Ti-MORB and low Ti-SSZ ophiolites (e.g. El Bahariya 2012, 2018). However, most recent studies are in favor of a supra-subduction zone setting, specifically in the fore-arc (Ali et al. 2020; Abdel-Karim et al. 2021; Moussa et al. 2021).

Because of metamorphism, the tectonic setting of igneous rock protoliths has to be inferred using elements immobile during metamorphism, including Ti, Zr, Y and Nb (e.g. Pearce and Cann 1973; Meschede 1986; Pearce 2008, 2014; Baziotis et al. 2014). In the Hf–Th–Nb diagram, the metagabbro samples plot in the destructive plate margin field (Fig. 8b). On the Th/Yb vs. Nb/Yb diagram (Pearce 2014), both the ophiolitic metapyroxenite and metagabbro plot above the MORB-OIB array toward the volcanic-arc array (Fig. 8c). Moreover, the metagabbro samples are relatively enriched in LREEs and LILEs, similar to magmatic rocks formed at convergent plate margins (e.g., Saunders et al. 1991; Hawkesworth et al. 1993). According to Geng et al. (2011), the metagabbro and metapyroxenite of the Al-Barramiya ophiolite have low Zr (35.88–42.60 ppm in metagabbro and 4.2–7.03 ppm in metapyroxenite), coupled with low

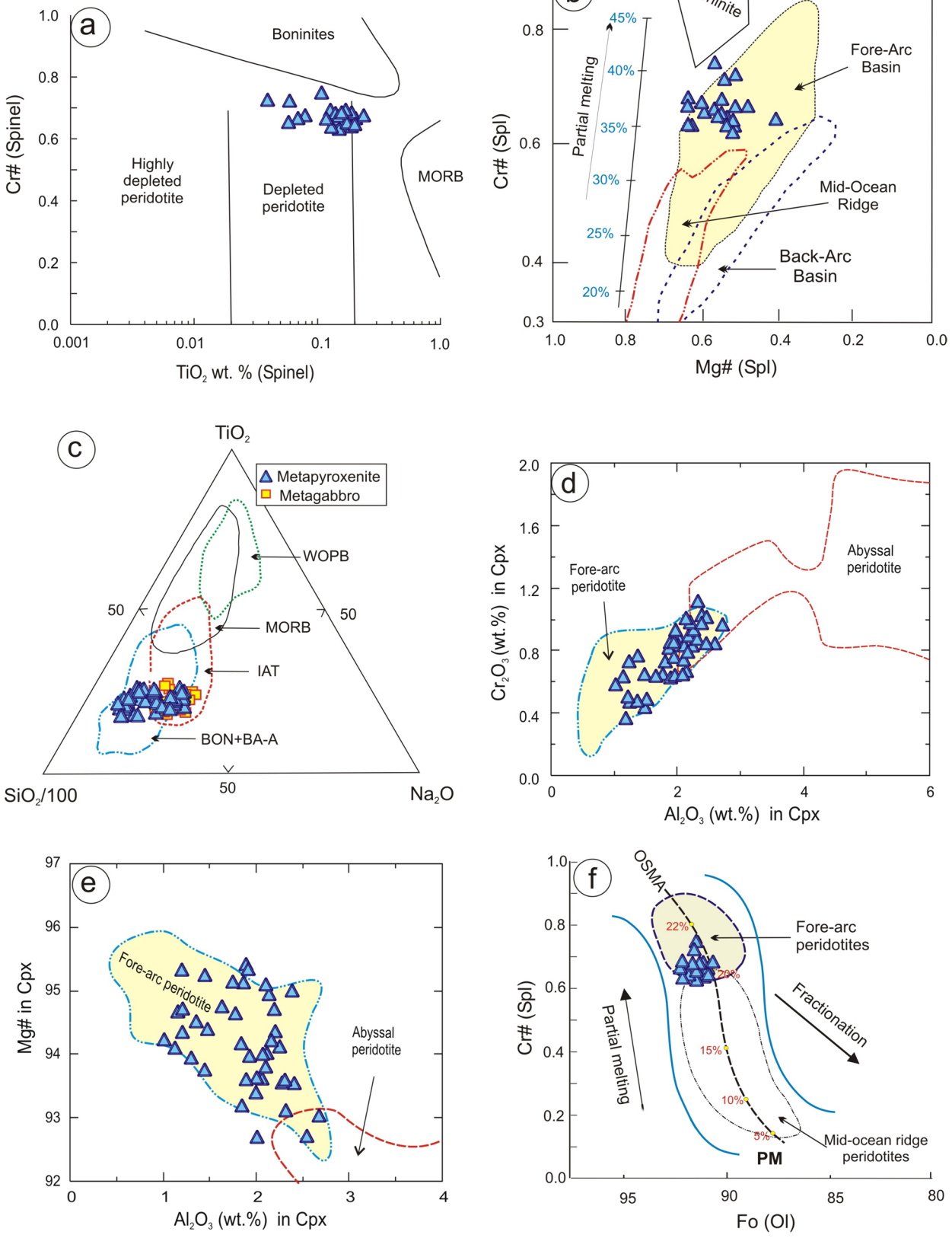
a
Boninites
Highly depleted peridotite
Depleted peridotite
MORB
Cr# (Spinel)
TiO2 wt. % (Spinel)
b
Boninite
Fore-Arc Basin
Mid-Ocean Ridge
Back-Arc Basin
Partial melting
45%
40%
35%
30%
25%
20%
Cr# (Spl)
Mg# (Spl)
c
TiO2
Metapyroxenite
Metagabbro
WOPB
MORB
IAT
BON+BA-A
50
SiO2/100
Na2O
d
Fore-arc peridotite
Abyssal peridotite
Cr2O3 (wt.%) in Cpx
Al2O3 (wt.%) in Cpx
e
Fore-arc peridotite
Abyssal peridotite
Mg# in Cpx
Al2O3 (wt.%) in Cpx
f
OSMA
22%
20%
15%
10%
5%
PM
Fore-arc peridotites
Fractionation
Partial melting
Mid-ocean ridge peridotites
Cr# (Spl)
Fo (Ol)

◂**Fig. 9** Tectonic discrimination diagrams for metagabbro and metapyroxenite based on mineral chemistry. **a** Cr# vs. TiO_2 diagram for fresh Cr-spinels in metapyroxenite. The fields are according to Dick and Bullen (1984), Jan and Windley (1990) and Arai (1992); **b** Cr# vs. Mg# diagram for fresh Cr-spinels (after Stern et al. 2004); the field boundaries are from Dick and Bullen (1984), Bloomer et al. (1995) and Ohara et al. (2002). The melting trend of experimental equilibrium (melting %) is from Hirose and Kawamoto (1995); **c** TiO_2–Na_2O–SiO_2/100 diagram for clinopyroxene in the metapyroxenite and metagabbro (after Beccaluva et al. 1989). WOPB within-ocean plate basalts, MORB mid-ocean ridge basalts, IAT island arc tholeiites, BON + BA–A boninites + basaltic andesites and andesites from intraoceanic fore-arcs; **d** Cr_2O_3 vs. Al_2O_3 diagram for clinopyroxene from the metapyroxenites; **e** Al_2O_3 vs. Mg# plot showing clinopyroxene from the metapyroxenite; and **f** Cr# vs. Fo for spinel coexisting with olivine in the metapyroxenites (olivine-spinel mantle array; OSMA); fields of fore-arc and mid-ocean ridge peridotites, and partial melting trend are from Arai (1994). Compositional fields for pyroxene in **b** and **c** are adopted from Pagé et al. (2008) and Xiong et al. (2018)

Nb (1.96–2.75 ppm in the metagabbro and 0.04–0.08 ppm in the metapyroxenite), indicating a depleted mantle source: our new data support this assertion. Furthermore, the Dy/Yb ratios (1.74–1.92 in metapyroxenite and 1.43–1.62 in metagabbro) and La/Yb ratios (0.41–0.55 in metapyroxenite and 2.36–2.70 in metagabbro) indicate up to 30% partial melting of a spinel lherzolite source (Fig. 8d).

The serpentinized clinopyroxenite has fresh relicts of primary silicates (e.g., olivine and pyroxene) and Cr-spinel, which are important petrogenetic indicators of the protolith (Barnes and Roeder 2001; Arif and Jan 2006). The very low TiO_2 content in the Cr-spinel from the metapyroxenite samples confirm their highly depleted character and indicate their association with SSZ tectonic settings. In residual peridotites, the Cr# of spinel reflects the degree of partial melting (Arai 1994). The high Cr# of spinel from the metapyroxenite samples therefore indicates a high degree of melting, as would be expected in the SSZ (Parkinson and Pearce 1998). Hence, on the Cr# versus TiO_2 plot the fresh Cr-spinel plots in the depleted field (Fig. 9a). The chemical composition of fresh Cr-spinel can be successfully used to distinguish between a back-arc and a fore-arc setting (Barnes and Roeder 2001; Ohara et al. 2002; Stern et al. 2004; Azer and Stern 2007 and many others), with the Cr# versus Mg# plot of fresh Cr-spinel in the serpentinized metapyroxenite indicating that most of the analysed Cr-spinels are similar to those of modern forearc peridotites (Fig. 9b).

In addition, clinopyroxene can provide further insight into the petrogenesis of the metapyroxenite from Al-Barramiya. Here, clinopyroxenes in the metapyroxenite and metagabbro plot in the fields of boninite and island-arc tholeiite (Fig. 9c), confirming the fore-arc setting, as boninite is endemic to fore-arcs (e.g., Bedard 1999; Beccaluva et al. 2004). Likewise, the clinopyroxene in the metapyroxenite is characterized by low Al_2O_3 contents, plotting in the field of fore-arc peridotites on the Cr_2O_3 versus Al_2O_3 and Mg# versus Al_2O_3 diagrams (Fig. 9d, e). In addition, clinopyroxene in the metapyroxenite has a Mg# (0.93–0.95) similar to those reported for ophiolitic pyroxenite [Mg# = 0.90–0.91 (Parlak et al. 1996); 0.86–0.91 (Whattam et al. 2011); 0.89–0.91 (Singh et al. 2017)] Furthermore, the negative correlation between Al_2O_3 and Mg# in the clinopyroxene (Supplementary table ST2) is similar to that reported for the ultramafic cumulates from the Troodos and Mersin ophiolites (Hébert and Laurent 1990; Parlak et al. 1996).

Fresh relicts of magmatic olivine are Fo-rich (0.91–0.93), indicating they have a mantle source and were residual after extensive melting, similar to forearc peridotites (e.g. Stern et al. 2004; Coish and Gardner 2004). The high Mg content of olivine (Fo) is similar to forearc peridotites investigated elsewhere in the ANS (e.g. Stern et al. 2004; Khalil et al. 2014; Obeid et al. 2016; Abuamarah 2020 and others), where the relationship between the Fo content and the Cr# of coexisting Cr-spinel displays a partial melting trend (Fig. 9f), supporting a residual origin (Arai 1994) that is a similar to forearc peridotites elsewhere in the world (e.g. Pearce et al. 2000).

Mantle pyroxenites have been interpreted as: (1) the product of melt and/or fluid interaction with peridotite (Garrido and Bodinier 1999; Bodinier et al. 2008; Marchesi et al. 2013; Laukert et al. 2014; Rogkala et al. 2017; Le Roux and Liang 2019); (2) cumulates of more primitive melts (Wilshire and Shervais 1975; Batanova et al. 2011); (3) metamorphosed products of recycled oceanic crust (Pearson et al. 1993; Barth et al. 2001; Morishita et al. 2003, 2004) or metamorphic segregations of peridotite (Dick and Sinton 1979); and (4) assimilation and fractional crystallization where olivine was assimilated by percolating melt, followed by in situ fractional crystallization of pyroxenes (Laukert et al. 2014). Cumulate and metamorphic origins for the Al-Barramiya pyroxenites are not in general agreement with field and petrographic evidence or with the mineral and whole-rock geochemistry. Also, the available data do not support assimilation and fractional crystallization for their formation. Recently, the melt/rock reaction model has become the most adopted model for pyroxenite formation (Akizawa et al. 2016; Saka et al. 2019; Xiong et al. 2020). According to this model, olivine in harzburgite wall-rock dissolves through interaction with a Si-enriched melt, causing pyroxene to precipitate (Garrido and Bodinier 1999; Bodinier et al. 2008; Marchesi et al. 2013; Laukert et al. 2014; Rogkala et al. 2017; Le Roux and Liang 2019). We consider that this model is most likely applicable to the ophiolitic rocks in the Al-Barramiya area, and illustrate this in Fig. 10. Here, we show the sequence of events for formation of the Al-Barramiya ophiolitic section due to fore-arc spreading and obduction of the ophiolite sequence.

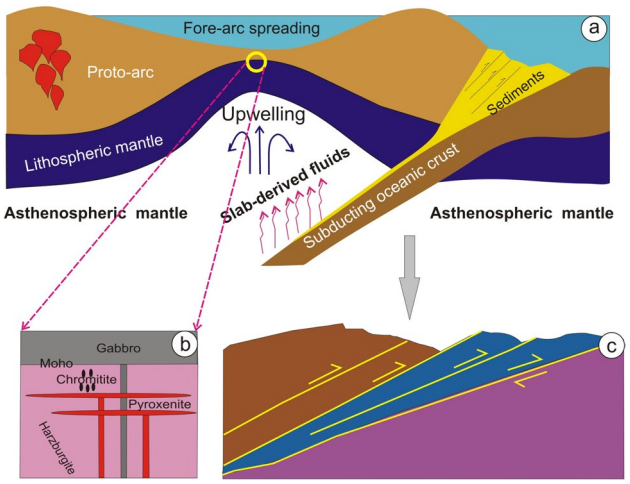

Fig. 10 Sequence of events for the formation of the Al-Barramiya ophiolite: **a** fore-arc spreading and formation of ophiolitic mantle section, **b** close-up of emplacement of pyroxenite and gabbro in the fore-arc, and **c** obduction of the ophiolite sequence resulting in brittle shear deformation

Conclusions

- The dismembered ophiolites in the Wadi Al-Barramiya area comprise serpentinized peridotite, metapyroxenite and metagabbro. The serpentinized peridotites are strongly altered to talc carbonate, magnesite and listvenite, but fresh relicts of primary minerals, including olivine and Cr-spinel, remain. The ophiolitic assemblage was metamorphosed under greenschist to lower amphibolite facies conditions.
- Ophiolitic metapyroxenite occurs as irregular coarse-grained lenses within serpentinite, whereas the metagabbros occur as scattered masses distributed throughout the ophiolitic mélange. Metapyroxenite is classified as websterite and olivine websterite and is mainly composed of altered clinopyroxene and serpentine, with fresh relicts of olivine, clinopyroxene and Cr-spinel. Metagabbro is comprised mainly of altered plagioclase, pyroxene, and amphibole.
- Metapyroxenite samples have low total REEs (3.52–5.69 ppm) and display LREE-depleted patterns [$(La/Sm)_n = 0.35–0.39$; $(La/Yb)n = 0.28–0.37$) accompanied by weakly fractionated HREE patterns ($Gd/Lu = 1.21–1.30$).
- The fresh Cr-spinel relicts in the metapyroxenite have high Cr# (0.63–0.75), which together with their low TiO_2 contents (0.04–0.24 wt%) are similar to highly refractory peridotites that evolve in fore-arcs. This is supported by the high forsterite content ($Fo = 0.91–0.93$) of fresh olivine and high Mg# (0.93–0.95) of fresh clinopyroxene.
- The metapyroxenite was formed as a magmatic rock derived from ultramafic magma at the base of the Neoproterozoic crust of the ANS due to melt-rock interaction, where olivine in harzburgite wall-rock dissolved through interaction with a Si-enriched melt, causing pyroxene to precipitate.
- Metagabbro samples are characterized by enrichment in LILE over HFSE and they are tholeiitic with a calc-alkaline affinity. They have flat REE patterns, with weak enrichment in LREE relative to HREE, and are similar to metagabbros associated with fore-arc ophiolites elsewhere in the ANS and around the world.

Supplementary Information The online version contains supplementary material available at https://doi.org/10.1007/s00531-024-02452-4.

Acknowledgements This work was supported by King Saud University (Researchers Supporting Project number RSP2024R151), which covered all analytical costs in Canada and China. We highly appreciate the efforts of the Editor-In-Chief (Prof. Ulrich Riller), Topic Editor (Prof. Timur Ustaomer) and the three reviewers (Prof. Ömer F. Çelik, Prof. Gaafar El Bahariya and anonymous) which greatly improved the manuscript.

Declarations

Conflict of interest The authors declare that the research was conducted in the absence of any commercial or financial relationships that could be construed as a potential conflict of interest.

References

Abd El-Rahman Y, Polat A, Dilek Y, Fryer B, El-Sharkawy M, Sakran S (2009a) Geochemistry and tectonic evolution of the Neoproterozoic Wadi Ghadir ophiolite, Eastern Desert, Egypt. Lithos 113(1–2):158–178

Abd El-Rahman Y, Polat A, Dilek Y, Fryer BJ, El-Sharkawy M, Sakran S (2009b) Geochemistry and tectonic evolution of the Neoproterozoic incipient arc-forearc crust in the Fawakhir area, Central Eastern Desert of Egypt. Precambrian Res 175:116–134

Abd El-Rahman Y, Helmy HM, Shibata T, Yoshikawa M, Arai S, Tamura A (2012) Mineral chemistry of the Neoproterozoic Alaskan-type Akarem Intrusion with special emphasis on amphibole: implications for the pluton origin and evolution of subduction-related magma. Lithos 155:410–425

Abdel Halim AHA, Helmy HM, Abd El-Rahman YM, Shibata T, El Mahallawi MM, Yoshikawa M, Arai S (2016) Petrology of the Motaghairat mafic–ultramafic complex, Eastern Desert, Egypt: a high-Mg post-collisional extension-related layered intrusion. J Asian Earth Sci 116:164–180

Abdel-Karim AM, Ali S, El-Shafei SA (2018) Mineral chemistry and geochemistry of ophiolitic metaultramafics from Um Halham and Fawakhir, Central Eastern Desert, Egypt. Int J Earth Sci 107:2337–2355

Abdel-Karim AM, El-Shafei SA, Azer MK (2021) The Neoproterozoic ophiolitic ultramafic rocks in Eastern Desert of Egypt: implications for petrogenesis and metasomatic processes. Int Geol Rev 63(2):208–232

Abuamarah BA (2020) Geochemistry and fore-arc evolution of upper mantle peridotites in the Cryogenian Bir Umq ophiolite, Arabian Shield, Saudi Arabia. Int Geol Rev 62(5):630–648

Abuamarah BA, Asimow PD, Azer MK, Ghrefat H (2020) Suprasubduction-zone origin of the podiform chromitites of the Bir Tuluhah ophiolite, Saudi Arabia, during Neoproterozoic assembly of the Arabian Shield. Lithos 360:105439

Abuamarah BA, Alshehri F, Azer MK, Asimow PD (2023) Geological and tectonic significance of rodingite in the Ess ophiolite, Arabian Shield, Saudi Arabia. Lithos 448:107168

Ahmed AH (2013) Highly depleted harzburgite–dunite–chromitite complexes from the Neoproterozoic ophiolite, south Eastern Desert, Egypt: a possible recycled upper mantle lithosphere. Precambrian Res 233:173–192

Ahmed AH, Arai S, Attia AK (2001) Petrological characteristics of podiform chromitites and associated peridotites of the Pan African ophiolite complexes of Egypt. Miner Depos 36:72–84

Ahmed AH, Gharib M, Arai S (2012) Characterization of the thermally metamorphosed mantle-crust transitionzone of the Neoproterozoic ophiolite at Gebel Mudarjaj, south Eastern Desert, Egypt. Lithos 142–143:67–83

Akaad MK, Noweir AM, Abu Ela AM, El Bahariya GA (1997) The Um Esh olistostromal mélange, Qift-Quseir region, central eastern desert, Egypt. Egypt J Geol 41:465–494

Akizawa N, Ozawa K, Tamura A, Michibayashi K, Arai S (2016) Three-dimensional evolution of melting, heat and melt transfer in ascending mantle beneath a fast-spreading ridge segment constrained by trace elements in clinopyroxene from concordant dunites and host harzburgites of the Oman ophiolite. J Petrol 57(4):777–814

Ali RAM, Pitcairn IK, Maurice AE, Azer MK, Bakhit BR, Shahien MG (2020) Petrology and geochemistry of ophiolitic ultramafic rocks and chromitites across the Eastern Desert of Egypt: insights into the composition and nature of a Neoproterozoic mantle and implication for the evolution of SSZ system. Precambrian Res 337:105565

Ali S, Azer M, Abdel-Karim AA (2023) Origin and evolution of Neoproterozoic metaophiolitic mantle rocks from the eastern Desert of Egypt: implications for tectonic and metamorphic events in the Arabian-Nubian Shield. Geol Acta 21:1–VII

Ali-Bik WM, Taman Z, El Kalioubi B, Abdel Wahab W (2012) Serpentinite-hosted talc–magnesite deposits of Wadi Barramiya area, Eastern Desert, Egypt: characteristics, petrogenesis and evolution. J Afr Earth Sci 64:77–89

Allahyari K, Saccani E, Rahimzadeh B, Zeda O (2014) Mineral chemistry and petrology of highly magnesian ultramafic cumulates from the Sarve-Abad (Sawlava) ophiolites (Kurdistan, NW Iran): new evidence for boninitic magmatism in intra-oceanic forearc setting in the Neo-Tethys between Arabia and Iran. J Asian Earth Sci 79:312–328

Arai S (1992) Chemistry of chromian spinel in volcanic rocks as a potential guide to magma chemistry. Mineral Mag 56:173–184

Arai S (1994) Characterization of spinel peridotites by olivine-spinel compositional relationships: review and interpretation. Chem Geol 113(3–4):191–204

Arai S, Shimizu Y, Ismail S, Ahmed A (2006) Low-T formation of high-Cr spinel with apparently primary chemical characteristics within podiform chromitite from Rayat, northeastern Iraq. Mineral Mag 70:499–508

Arif M, Jan MQ (2006) Petrotectonic significance of the chemistry of chromite in the ultramafic-mafic complexes of Pakistan. J Asian Earth Sci 27:628–646

Azer MK, Stern RJ (2007) Neoproterozoic (835–720 Ma) serpentinites in the Eastern Desert, Egypt: fragments of fore-arc mantle. Geol J 115:457–472

Azer MK, Gahlan HA, Asimow PD, Al-Kahtany KM (2017) The late Neoproterozoic Dahanib mafic-ultramafic intrusion, South eastern Desert, Egypt: is it an Alaskan-type or a layered intrusion? Am J Sci 317(8):901–940

Azer MK, Gahlan HA, Asimow PD, Mubarak HS, Al-Kahtany KM (2019) Multiple stages of carbonation and element redistribution during formation of ultramafic-hosted magnesite in Neoproterozoic ophiolites of the Arabian-Nubian Shield, Egypt. J Geol 127:81–107

Azer MK, Samuel MD, Ali KA, Gahlan HA, Stern RJ, Ren M, Moussa HE (2013) Neoproterozoic ophiolitic peridotites along the Allaqi-Heiani Suture, South Eastern Desert, Egypt. Mineral Petrol 107:829–848

Bahrambeygi B, Moeinzadeh H, Alavipanah S (2019) Mineralogy, geochemistry and raman spectroscopy of multi-genesis serpentine polymorphs of Darepahn ophiolites. J Sci Islam Rep Iran 30(3):251–269

Barnes SJ (2000) Chromite in komatiites, II. Modification during greenschist to mid-amphibolite facies metamorphism. J Petrol 41:387–409

Barnes SJ, Roeder PL (2001) The range of spinel compositions in terrestrial mafic and ultramafic rocks. J Petrol 42(12):2279–2302

Barrert TJ, MacLean WH (1994) Chemostratigraphy and hydrothermal alteration in exploration for VHMS deposits in greenstone and younger volcanic rocks. In: Lenz DR (ed) Alteration processes associated with ore-forming systems. Geol. Assoc. Canada, short course notes, vol 11, pp 433–467

Barth MG, Rudnick RL, Horn I, McDonough WF, Spicuzza MJ, Valley JW, Haggerty SE (2001) Geochemistry of xenolithic eclogites from West Africa, Part I: a link between low MgO eclogites and Archean crust formation. Geochim Cosmochim Acta 65(9):1499–1527

Basta FF, Maurice AE, Bakhit BR, Ali KA, Manton WI (2011) Neoproterozoic contaminated MORB of Wadi Ghadir Ophiolite, NE Africa: geochemical and Nd and Sr isotopic constraints. J Afr Earth Sci 59:227–242

Batanova VG, Belousov IA, Savelieva GN, Sobolev AV (2011) Consequences of channelized and diffuse melt transport in suprasubduction zone mantle: evidence from the Voykar Ophiolite (Polar Urals). J Petrol 52(12):2483–2521

Baziotis I, Mposkos E, Asimow PD (2014) Continental rift and oceanic protoliths of mafic–ultramafic rocks from the Kechros Complex, NE Rhodope (Greece): implications from petrography, major and trace-element systematics, and Melts modeling. Int J Earth Sci 103(4):981–1003

Beccaluva L, Macciotta G, Piccardo GB, Zeda O (1989) Clinopyroxene composition of ophiolite basalts as petrogenetic indicator. Chem Geol 77:165–182

Beccaluva L, Coltori M, Giunta G, Siena F (2004) Tethyan vs. Cordilleran ophiolites: a reappraisal of distinctive tectono-magmatic features of supra-subduction complexes in relation to subduction mode. Tectonophysics 393:163–174

Bédard JH (1999) Petrogenesis of boninites from the Betts Cove ophiolite, Newfoundland, Canada: identification of subducted source components. J Petrol 40:1853–1889

Bloomer S, Taylor B, MacLeod C, Stern R, Fryer P, Hawkins J, Johnson L (1995) Early arc volcanism and ophiolite problem: a perspective from drilling in the Western Pacific. In: Taylor B, Natland J (eds) Active margins and marginal basins of the Western Pacific, geophysical monograph. American Geophysical Union. Washington DC, vol 88, pp 1–30

Bodinier JL, Godard M (2003) Orogenic, ophiolitic, and abyssal peridotites. Treatise Geochem 2:568

Bodinier JL, Garrido CJ, Chanefo I, Bruguier O, Gervilla F (2008) Origin of pyroxenite–peridotite veined mantle by refertilization reactions: evidence from the Ronda peridotite (Southern Spain). J Petrol 49(5):999–1025

Boskabadi A, Pitcairn IK, Broman C, Boyce A, Teagle DAH, Cooper MJ, Azer MK, Stern RJ, Mohamed FH, Majka J (2017) Carbonate alteration of ophiolitic rocks in the Arabian-Nubian Shield of Egypt: sources and compositions of the carbonating fluid and implications for the formation of Au deposits. Int Geol Rev 59(4):391–419

Coish RA, Gardner P (2004) Suprasubduction-zone peridotite in the northern USA Appalachians: evidence from mineral composition. Mineral Mag 68:699–708

Coleman RG (1977) Ophiolites. Springer, Berlin, p 229

Cox KG, Bell JD, Pankhurst RJ (1979) Compositionally zoned magma bodies and their bearing on crystal settling. In: The interpretation of igneous rocks. Springer, Dordrecht, pp 272–282

Deer WA, Howie RA, Zussman J (1992) An introduction to the rock forming minerals, 2nd edn. Longman Scientific and Technical, London

Dick HJ, Bullen T (1984) Chromian spinel as a petrogenetic indicator in abyssal and alpine-type peridotites and spatially. Contrib Mineral Petrol 86(1):54–76

Dick HJB, Sinton JM (1979) Compositional layering in alpine peridotites: evidence for pressure solution creep in the mantle. Geol J 87:403–416

Dilek Y, Furnes H (2014) Ophiolites and their origins. Elements 10(2):93–100

El Bahariya GA (2006) Petrology, mineral chemistry and metamorphism of two pan-African ophiolitic metagabbro occurrences, Central Eastern Desert, Egypt. Egypt J Geol 50:183–202

El Bahariya GA (2008) Geology, mineral chemistry and petrogenesis of Neoproterozoic metamorphosed ophiolitic ultramafics, Central Eastern Desert, Egypt: implications for the classification and origin of the ophiolitic mélange. Egypt J Geol 52:55–82

El Bahariya GA (2012) Classification and origin of the Neoproterozoic ophiolitic mélanges in the Central Eastern Desert of Egypt. Tectonophysics 568:357–370

El Bahariya G (2018) Classification of the Neoproterozoic ophiolites of the Central Eastern Desert, Egypt based on field geological characteristics and mode of occurrence. Arab J Geosci 11:1–23

El Bahariya G.A, Arai S (2003) Petrology and origin of Pan-African serpentinites with particular reference to chromian spinel compositions, Eastern Desert, Egypt: implication for supra-subduction zone ophiolite. In: Third international conference on the geology of Africa, Assiut University, Egypt, pp 371–388

El Sharkawy MA, El Bayoumi RM (1979) The ophiolites of Wadi Ghadir area, Eastern Desert, Egypt. Ann Geol Surv Egypt 9:125–135

Evans BW (2010) Lizardite vs. antigorite serpentinite: magnetite, hydrogen, and life (?). Geology 38:879–882

Evans BW, Frost BR (1975) Chrome-spinel in progressive metamorphism—a preliminary analysis. Geochim Cosmochim Acta 39:959–972

Farahat ES (2008) Chrome-spinels in serpentinites and talc carbonates of the El Ideid-El-Sodmein District, central Eastern Desert, Egypt: their metamorphism and petrogenetic implications. Chem Erde 68:193–205

Franz L, Wirth R (2000) Spinel inclusions in olivine of peridotite xenoliths from TUBAF seamount (Bismarck Archipelago/Papua New Guinea): evidence for the thermal and tectonic evolution of the oceanic lithosphere. Contrib Mineral Petrol 140(3):283–295

Gahlan HA, Arai S, Abu El-Ela FF, Tamura A (2012) Origin of wehrlite cumulates in the Moho transition zone of the Neoproterozoic Ras Salatit ophiolite, Central Eastern Desert, Egypt: crustal wehrlites with typical mantle characteristics. Contrib Mineral Petrol 163:225–241

Gahlan HA, Azer MK, Khalil AE (2015) The neoproterozoic Abu Dahr ophiolite, South Eastern Desert, Egypt: petrological characteristics and tectonomagmatic evolution. Mineral Petrol 109:611–630

Gahlan HA, Azer MK, Asimow PD (2018) On the relative timing of listwaenite formation and chromian spinel equilibration in serpentinites. Am Minerol 103:1087–1102

Gahlan HA, Azer MK, Asimow PD, Mubarak HS, Al-Kahtany KM (2020) Petrological characteristics of the Neoproterozoic Ess ophiolite mantle section, Arabian Shield, Saudi Arabia: a mineral chemistry perspective. Int J Earth Sci 109:239–251

Gahlan HA, Azer MK, Al-Kahtany KM (2021) Petrogenesis and geodynamic setting of high-Cr chromitites in fore-arc peridotites: a case study from the Halaban ophiolite, Eastern Arabian Shield, Saudi Arabia. Lithos 396:106243

Gahlan HA, Azer MK, Al-Hashim MH, Osman MS (2023) New insights and constraints on the late Neoproterozoic post-collisional mafic magmatism in the Arabian Shield, Saudi Arabia. Lithos 436:106989

Garrido CJ, Bodinier JL (1999) Diversity of mafic rocks in the Ronda peridotite: evidence for pervasive melt–rock reaction during heating of subcontinental lithosphere by upwelling asthenosphere. J Petrol 40(5):729–754

Geng H, Sun M, Yuan C, Zhao G, Xiao W (2011) Geochemical and geochronological study of early Carboniferous volcanic rocks from the West Junggar: petrogenesis and tectonic implications. J Asian Earth Sci 42(5):854–866

Hawkesworth CJ, Gallagher K, Hergt JM, McDermott F (1993) Mantle and slab contributions in arc magmas. Annu Rev Earth Planet Sci 21(1):175–204

Hawthorne FC, Oberti R, Harlow GE, Maresch WV, Martin RF, Schumacher JC, Welch MD (2012) Nomenclature of the amphibole supergroup. Am Minerol 97(11–12):2031–2048

Hébert R, Laurent R (1990) Mineral chemistry of the plutonic section of the Troodos ophiolite: new constraints for genesis of arc-related ophiolites. In: Malpas J, Moores E, Panayiotou A, Xenophontos C (eds) Ophiolites–oceanic crustal analogues. In: Proceedings of Troodos Ophiolite symposium 1987, Nicosia, Cyprus Geological Survey, pp 149–116

Helmy HM, El Mahallawi MM (2003) Gabbro Akarem mafic-ultramafic complex, Eastern Desert, Egypt: a Late Precambrian analogue of Alaskan-type complexes. Mineral Petrol 77:85–108

Hey MH (1954) A new review of the chlorites. Mineral Mag J Mineral Soc 30(224):277–292

Hirose K, Kawamoto T (1995) Hydrous partial melting of lherzolite at 1 GPa: the effect of H_2O on the genesis of basaltic magmas. Earth Planet Sci Lett 133:463–473

Irvine TN, Baragar WRA (1971) A guide to the chemical classification of the common volcanic rocks. Can J Earth Sci 8(5):523–548

Jan MQ, Windley BF (1990) Chromian spinel silicate chemistry in ultramafic rocks of the Jijal Complex, northwestern Pakistan. J Petrol 31:667–715

Khalil AES, Azer MK (2007) Supra-subduction affinity in the Neoproterozoic serpentinites in the Eastern Desert, Egypt: evidence from mineral composition. J Afr Earth Sci 49(4–5):136–152

Khalil AES, Obeid MA, Azer MK (2014) Serpentinized peridotites at the north part of Wadi Allaqi district (Egypt): implications for the tectono-magmatic evolution of fore-arc crust. Acta Geol Sin 88(Issue 5):1421–1436

Khedr MZ, Arai S (2017) Peridotite-chromitite complexes in the Eastern Desert of Egypt: insight into Neoproterozoic sub-arc mantle processes. Gondwana Res 52:59–79

Laukert G, Von Der Handt A, Hellebrand E, Snow JE, Hoppe P, Klügel A (2014) High-pressure reactive melt stagnation recorded in abyssal pyroxenites from the ultraslow-spreading Lena Trough. Arctic Ocean J Petrol 55(2):427–458

Le Bas MJ (1962) The role of aluminum in igneous clinopyroxenes with relation to their parentage. Am J Sci 260:267–288

Le Roux V, Liang Y (2019) Ophiolitic pyroxenites record boninite percolation in subduction zone mantle. Minerals 9(9):565

Lindsley DH (1983) Pyroxene thermometry. Am Minerol 68:477–493

Marchesi C, Garrido CJ, Bosch D, Bodinier JL, Gervilla F, Hidas K (2013) Mantle refertilization by melts of crustal-derived garnet pyroxenite: evidence from the Ronda peridotite massif, southern Spain. Earth Planet Sci Lett 362:66–75

McDonough WF, Sun SS (1995) The composition of the Earth. Chem Geol 120(3–4):223–253

Mellini M, Rumori C, Viti C (2005) Hydrothermally reset magmatic spinels in retrograde serpentinites: formation of "ferritchromit" rims and chlorite aureoles. Contrib Mineral Petrol 149:266–275

Meschede M (1986) A method of discriminating between different types of mid-ocean ridge basalts and continental tholeiites with the Nb 1bZr 1bY diagram. Chem Geol 56(3–4):207–218

Moody JB (1976) Serpentinization: a review. Lithos 9:125–138

Morimoto N, Fabries J, Ferguson AK, Ginzburg IV, Ross M, Seifert FA, Zussman J (1988) Nomenclature of pyroxenes. Mineral Mag 52:535–550

Morishita T, Arai S, Green DH (2003) Evolution of low-Al orthopyroxene in the Horoman peridotite, Japan: an unusual indicator of metasomatizing fluids. J Petrol 44(7):1237–1246

Morishita T, Arai S, Green DH (2004) Possible non-melted remnants of subducted lithosphere: experimental and geochemical evidence from corundum-bearing mafic rocks in the Horoman Peridotite Complex. Jpn J Petrol 45(2):235–252

Moussa HE, Azer MK, Abou El Maaty MA, Maurice AE, Yanni NN, Akarish AI, Elnazer AA, Elsagheer MA (2021) Carbonation of Neoproterozoic mantle section and formation of gold-bearing listvenite in the Northern Nubian Shield. Lithos 406:106525

Moussa HE, Mubarak HS, Azer MK, Surour AA, Asimow PD, Kabesh MM (2022) Multistage petrogenetic evolution of Neoproterozoic serpentinized ultramafic rocks and podiform chromitites at Hagar Dungash, Eastern Desert of Egypt. Precambrian Res 369:106507

Nozaka T (2010) A note on compositional variation of olivine and pyroxene in thermally metamorphosed ultramafic complexes from SW Japan. Okayama University. Earth Sci Res 17:1–5

Obeid MA, Khalil AE, Azer MK (2016) Mineralogy, geochemistry, and geotectonic significance of the Neoproterozoic ophiolite of Wadi Arais area, south Eastern Desert, Egypt. Int Geol Rev 58(6):687–702

Ohara Y, Stern RJ, Ishii T, Yurimoto H, Yamazaki T (2002) Peridotites from the Mariana Trough: first look at the mantle beneath an active back-arc basin. Contrib Mineral Petrol 143(1):1–18

Pagé P, Bédard J, Schroetter J, Tremblay A (2008) Mantle petrology and mineralogy of the Thetford Mines ophiolite complex. Lithosphere 100:255–292

Parkinson IJ, Pearce JA (1998) Peridotites from the Izu–Bonin–Mariana forearc (ODP Leg 125): evidence for mantle melting and melt–mantle interaction in a supra-subduction zone setting. J Petrol 39(9):1577–1618

Parlak O, Delaloye M, Bíngöl E (1996) Mineral chemistry of ultramafic and mafic cumulates as an indicator of the arc-related origin of the Mersin ophiolite (southern Turkey). Geol Rundsch 85(4):647–661

Parlak O, Höck V, Delaloye M (2000) Suprasubduction zone origin of the Pozanti-Karsanti ophiolite (southern Turkey) deduced from whole-rock and mineral chemistry of the gabbroic cumulates. Geol Soc Lond Spec Publ 173(1):219–234

Parlak O, Karaoğlan F, Rizaoğlu T, Nurlu N, Bağci U, Höck V, Öztüfekçi Önal A, Kürüm A, Topak Y (2013) Petrology of the İspendere (Malatya) ophiolite from the Southeast Anatolia: Implications for the Late Mesozoic evolution of the southern Neotethyan Ocean. Geol Soc Lond Spec Publ 372(1):219–247

Pearce JA (2008) Geochemical fingerprinting of oceanic basalts with applications to ophiolite classification and the search for Archean oceanic crust. Lithos 100(1–4):14–48

Pearce JA (2014) Immobile elements fingerprinting of ophiolites. Elements 10(2):101–108

Pearce JA, Cann JR (1973) Tectonic setting of basic volcanic rocks determined using trace element analyses. Earth Planet Sci Lett 19(2):290–300

Pearce JA, Peate DW (1995) Tectonic implications of the composition of volcanic arc magmas. Annu Rev Earth Planet Sci 23:251–286

Pearce JA, Barker PF, Edwards SJ, Parkinson IJ, Leat PT (2000) Geochemistry and tectonic significance of peridotites from the South Sandwich arc-basin system, South Atlantic. Contrib Mineral Petrol 139:36–53

Pearson DG, Davies GR, Nixon PH (1993) Geochemical constraints on the petrogenesis of diamond facies pyroxenites from the Beni Bousera peridotite massif, North Morocco. J Petrol 34(1):125–172

Proenza JA, Ortega-Gutiérrez F, Camprubı A, Tritlla J, Elıas-Herrera M, Reyes-Salas M (2004) Paleozoic serpentinite-enclosed chromitites from Tehuitzingo (Acatlán Complex, southern Mexico): a petrological and mineralogical study. J S Am Earth Sci 16(8):649–666

Purvis AC, Nesbitt RW, Hallberg JA (1972) The geology of part of the Carr Boyd Rocks Complex and its associated nickel mineralization, Western Australia. Econ Geol 67(8):1093–1113

Rogkala A, Petrounias P, Tsikouras B, Hatzipanagiotou K (2017) New occurrence of pyroxenites in the Veria-Naousa ophiolite (north Greece): implications on their origin and petrogenetic evolution. Geosciences 7(4):92

Said A (2006) Petrology and structure of the Barramiya area with special emphasis on the gold mineralization, Eastern Desert, Egypt. M.Sc. Thesis, Faculty of Science, Cairo University, p 167

Saka S, Uysal I, Kapsiotis A, Bağcı U, Ersoy EY, Su BX, Seitz HM, Hegner E (2019) Petrological characteristics and geochemical compositions of the Neotethyan Mersin ophiolite (southern Turkey): processes of melt depletion, refertilization, chromitite formation and oceanic crust generation. J Asian Earth Sci 176:281–299

Salem AKA, Khalil AE, Ramadan TM (2012) Geology, geochemistry and tectonic setting of Pan-African serpentinites of Um Salim-Um Salatit area, Central Eastern Desert, Egypt. Egypt J Remote Sens Space Sci 15:171–184

Saunders AD, Norry MJ, Tarney J (1991) Fluid influence on the trace element compositions of subduction zone magmas. Philos Trans R Soc Lond Ser A Phys Eng Sci 335(1638):377–392

Shackleton RM (1994) Review of Late Proterozoic sutures, ophiolitic mélanges and tectonics of eastern Egypt and north-east Sudan. Geol Rundsch 83(3):537–546

Shackleton RM, Ries AC, Graham RH, Fitches WR (1980) Late Precambrian ophiolitic mélange in the Eastern Desert of Egypt. Nature 285(5765):472–474

Singh AK, Nayak R, Khogenkumar S, Subramanyam KSV, Thakur SS, Bikramaditya Singh RK, Satyanarayanan M (2017) Genesis and tectonic implications of cumulate pyroxenites and tectonite peridotites from the Nagaland-Manipur ophiolites, Northeast India: constraints from mineralogical and geochemical characteristics. Geol J 52(3):415–436

Stern RJ, Johnson PR, Kröner A, Yibas B (2004) Neoproterozoic ophiolites of the Arabian-Nubian shield. Dev Precambrian Geol 13:95–128

Suita M, Strieder A (1996) Cr-spinels from Brazilian mafic-ultramafic complexes: metamorphic modifications. Int Geol Rev 38:245–267

Takahashi E, Uto K, Schilling JG (1987) Primary magma compositions and Mg/Fe ratios of their mantle residues along mid-Atlantic ridge 29N to 73N. Technical report A9. Institute of Studies Earth's Interior, Okayama University Series, pp 1–14

Whattam SA, Cho M, Smith IE (2011) Magmatic peridotites and pyroxenites, Andong Ultramafic Complex, Korea: geochemical evidence for supra-subduction zone formation and extensive melt–rock interaction. Lithos 127(3–4):599–618

Whattam SA, De Hoog JC, Leybourne MI, Khedr MZ (2022) Link between melt-impregnation and metamorphism of Atlantis Massif peridotite (IODP Expedition 357). Contrib Mineral Petrol 177(11):106

Wilshire HG, Shervais JW (1975) Al–augite and Cr–diopside ultramafic xenoliths in basaltic rocks from western United States. In: Physics and chemistry of the Earth. Pergamon, pp 257–272

Wilson M (1989) Igneous petrogenesis: a global tectonic approach. Unwin Hyman, London

Wood DA (1980) The application of a Th-Hf-Ta diagram to problems of tectonomagmatic classification and to establishing the nature of crustal contamination of basaltic lavas of the British Tertiary Volcanic Province. Earth Planet Sci Lett 50(1):11–30

Xiong F, Yang J, Dilek Y, Wang C, Hao X, Xu X, Lian D (2018) Petrology and geochemistry of the high-Cr podiform chromitites of the Köycegiz ophiolite, southwest Turkey: implications for the multi-stage evolution of the oceanic upper mantle. Mineral Petrol 112:685–704

Xiong F, Dilek Y, Wirth R, Xu X, Yang J (2020) Opx-Cpx exsolution textures in lherzolites of the Cretaceous Purang Ophiolite (S. Tibet, China), and the deep mantle origin of Neotethyan abyssal peridotites. Int Geol Rev 62(6):665–682

Xu YG, Menzies MA, Thirlwall MF, Xie GH (2001) Exotic lithosphere mantle beneath the western Yangtze craton: petrogenetic links to Tibet using highly magnesian ultrapotassic rocks. Geology 29(9):863–866

Zimmer M, Kröner A, Jochum KP, Reischmann T, Todt W (1995) The Gabal Gerf complex: a Precambrian N-MORB ophiolite in the Nubian Shield, NE Africa. Chem Geol 123:29–51

Zoheir BA, Lehmann B (2011) Listvenite-lode association at the Barramiya gold mine, Eastern Desert, Egypt. Ore Geol Rev 39:101–115